Chapter 10
Plasma Applications

10.1 Introduction

The effect of plasmas had been noticed as early as 1901, when Marconi found that radio waves could cross the Atlantic in spite of the curvature of the earth. We now know that the waves were reflected by the ionosphere. The study of plasmas probably began with Irving Langmuir's experiments on sheaths in 1928, and it was he who coined the name plasma in a blood-free context. Practical use of plasmas began in the late 1940s with E.O. Lawrence's invention of the calutron (named for the University of California) for the separation of U^{235} from U^{238} for use in atomic bombs. It was the effort to tame the H-bomb into a steady source of electricity—hydrogen fusion—that spawned modern plasma physics. More on that later.

Today, many objects used in everyday life are made or treated with plasmas. These are not the fully ionized plasmas needed for fusion but are partially ionized plasmas with electron temperatures below about 4 eV, the so-called low-temperature plasmas. About 12 % of electricity generated in the U.S. is used for lighting, and over 60 % of lamps involve low-temperature plasmas. Fluorescent lights use an argon or neon plasma containing mercury to generate invisible ultraviolet light, which then excites a phosphor coating that glows visibly. Fluorescents are being replaced by more efficient LEDs (light-emitting diodes), which contain solid-state plasmas in *p-n* junctions. The latter are also at the heart of solar cells. Semiconductors in electronic devices are made with the use of plasma etching and deposition. Plastic sheets are made hydrophylic or hydrophobic depending on whether they are to be printed on, such as in food packaging. The pixels in our TVs and computer screens are etched with plasmas. Windows are glazed with plasmas to transmit or reflect specific wavelengths. Heat barriers in jet engines are made with plasma deposition. Thrusters in spacecraft are plasma ejectors (Sect. 10.4). In

The original version of this chapter was revised. An erratum to this chapter can be found at https://doi.org/10.1007/978-3-319-22309-4_11

F.F. Chen, *Introduction to Plasma Physics and Controlled Fusion*,
DOI 10.1007/978-3-319-22309-4_10

medicine, plasmas are used for sterilization and for hardening or knee implants by ion implantation, for instance. The subject of plasma chemistry has been developed for these applications. All lasers contain plasmas, ranging from the huge megajoule lasers at Livermore in the U.S., in Osaka in Japan, and at Bordeaux in France, to the laser pointers used in lectures.

Many phenomena in basic physics either involve plasmas or may involve plasmas when finally solved. Lightning strikes are gas discharges between charged clouds or between a cloud and ground. Ball lightning is a glowing sphere of plasma that is on the ground and lasts many seconds. Because of its unpredictability, it is unexplained. The geodynamo inside the earth that creates its magnetic field involves motions of liquids, but probably not gaseous plasmas. The BICEP2 experiment (Background Imaging of Cosmic Extragalactic Polarization) seeks to find evidence of primordial gravitational waves from the Big Bang in the cosmic microwave background. Dust is believed to be involved. Dusty plasmas have been added to this edition.

10.2 Fusion Energy

All of the world's energy depends on the sun. Our fossil fuels come from trees that grew in sunlight millions of years ago. Sunlight causes evaporation and makes clouds, and the rain or snow from them gives us hydropower. To minimize the CO_2 released by burning coal, oil, or gas, efforts are made to develop solar and wind power, both of which derive energy from the sun. The temperature in the sun's interior is about 1 keV. At this temperature hydrogen atoms live for a million years before they fuse into helium to release energy. What if we can make our own miniature sun on Earth? We can't wait a million years, so we must increase the temperature to speed up the process. We can also increase the inertia in a head-on collision with heavier isotopes: deuterium (D) with one proton and one neutron, and tritium (T) with one proton and two neutrons. The inertia has to overcome the electric repulsion of ions with like charges. For the sun, Hans Bethe invented the carbon cycle, in which protons can be made to fuse in a series of reactions involving carbon, each of which requires less energy. Better carbon cycles have been found since then, but no one has found a cycle that can work on our time scales. One might think that we could accelerate deuterons in a particle accelerator and put a solid piece of tritium ice in the beam, but that won't work because the deuterons lose more energy in off-angle scatters than they gain in head-on fusion collisions. There are two main ways to recover the energy from D–T fusion collisions: magnetic confinement, and inertial fusion.

10.2.1 Magnetic Fusion

By trapping a plasma in a magnetic field, the ions and electrons are in thermal equilibrium with Maxwellian distributions, so that the energy gained or lost in elastic collisions is returned to the thermal distribution. Only a few collisions result

in fusion. The idea is to create a 50–50 % DT plasma at around 30 keV so that there are enough high-energy ions in the tail of the distribution to fuse, generating more than the energy used to create the plasma. Since the plasma is in thermal equilibrium, these are called *thermonuclear reactions*. There are other nuclei besides D and T that can be used; the principal reactions are:

$$\begin{aligned}
&\mathrm{D} + \mathrm{T} \rightarrow \alpha + \mathrm{n} + 17.6\,\mathrm{MeV}\\
&\mathrm{D} + \mathrm{D} \rightarrow {}^{3}\mathrm{He} + \mathrm{n} + 3.27\,\mathrm{MeV}\\
&\mathrm{D} + \mathrm{D} \rightarrow \mathrm{T} + \mathrm{p} + 4.05\,\mathrm{MeV}\\
&\mathrm{D} + {}^{3}\mathrm{He} \rightarrow \alpha + \mathrm{p} + 18.34\,\mathrm{MeV}\\
&\mathrm{D} + {}^{6}\mathrm{Li} \rightarrow 2\alpha + 22.4\,\mathrm{MeV}\\
&\mathrm{p} + {}^{7}\mathrm{Li} \rightarrow 2\alpha + 17.2\,\mathrm{MeV}\\
&\mathrm{p} + {}^{6}\mathrm{Li} \rightarrow \alpha + {}^{3}\mathrm{He} + 4.0\,\mathrm{MeV}\\
&\mathrm{p} + {}^{11}\mathrm{B} \rightarrow 3\alpha + 8.7\,\mathrm{MeV}
\end{aligned}$$

Here *p* is a proton and *n* a neutron. The two D–D reactions occur with about equal probability, but one of them yields a neutron. Since thick shielding would be required to protect personnel from neutrons, aneutronic reactions are much preferred. Furthermore, neutrons not only require shielding but they also carry most of the energy, which must be captured as heat to be used in a steam turbine to produce electricity. The D–^{3}He reaction is aneutronic, but ^{3}He does not occur naturally. It is produced in the first D–D reaction, which is neutronic. The ^{6}Li reactions use the 8 % isotope of lithium. The p-^{7}Li reaction is aneutronic, but it occurs only 20 % of the time. This leaves the p-^{11}B reaction, which is the best choice because it is entirely aneutronic and ^{7}Li is a plentiful element. Though its reactivity is relatively low, p-^{11}B has such promise that it is being pursued by a private enterprise. Charged products can, in principle at least, produce electricity without going through a Carnot cycle.

Figure 10.1 shows the fusion probability for the various reactions. It is clear that the D–T reaction is by far the best. Shown in Fig. 10.2, the D–T reaction produces a neutron and a helium nucleus, or α-particle. The mass difference between the D + T and the resulting α + n is converted into 17.6 MeV of energy by $E = Mc^2$. Most of the energy is carried off by the 14-MeV neutron, while the 3.5-MeV α-particle is trapped in the magnetic field which confines the plasma. This confinement is far from perfect, and the mean times for leakage of ions and of plasma energy are called respectively τ_p and τ_E. Neglecting the difference between τ_p and τ_E, we show in Fig. 10.3 the required $n\tau$ product for breakeven and ignition. Breakeven occurs when the fusion energy produced is equal to that used in creating the plasma. This is called the *Lawson criterion*. Ignition occurs when the α-particles are trapped in the B-field long enough that they can maintain the plasma's temperature without further input of energy. The Joint European Tokamak (JET) in England is, at the time of this writing, on the verge of achieving breakeven. The ITER tokamak in France (originally an acronym of International Thermonuclear Experimental Reactor), is designed to achieve ignition some years after it begins D–T operation in 2027.

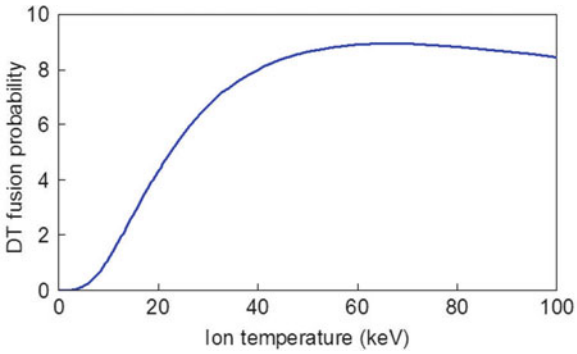

Fig. 10.1 Reactivity of various fusion collisions vs. ion temperature

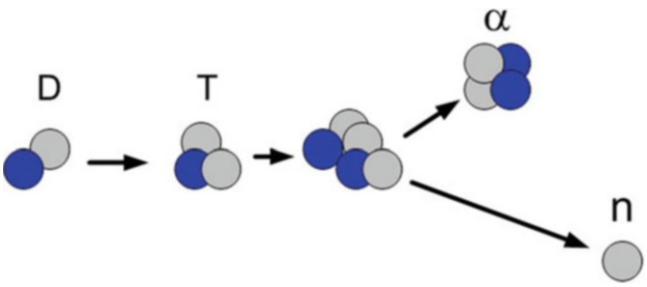

Fig. 10.2 Diagram of the D–T reaction

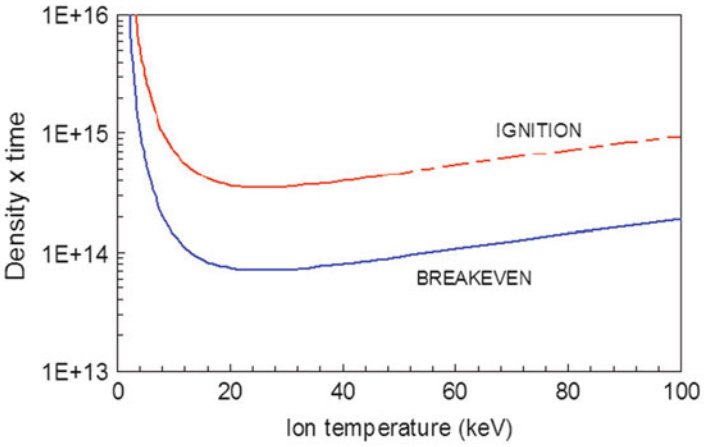

Fig. 10.3 The $n\tau$ product for D–T fusion, in units of cm^{-3} s, vs. KT_i

There are two principal ways to surpass the Lawson criterion: magnetic confinement and inertial confinement. In magnetic confinement, the minimum $n\tau$ in Fig. 10.3 is achieved by holding a dense plasma in a magnetic field for a time τ. In inertial confinement, a much denser plasma is held for a very short time by

compressing it with a laser or other pulsed power source. We consider magnetic confinement first. Ions and electrons gyrate in Larmor orbits but are free to move along lines of **B**. To trap them, one can use magnetic mirrors or cusps (see Figs. 2.7, 2.8, and 2.14), or close the lines in a torus. Large mirror machines have been built with special devices to slow the loss of particles which scatter into the loss cone, but these have not been as successful as tori. In a torus, the B-field lines must not close on themselves but must randomly trace out magnetic surfaces. Instabilities then arise, such as the gravitational instability in Sect. 6.7 and the drift-wave instability in Sect. 6.8. The former is driven by centrifugal force, and the latter by the pressure gradient which must exist somewhere in a confined plasma. An ion temperature gradient instability has also been troublesome. These instabilities have been brought under control by shear in the magnetic field and other more subtle means, and it is now possible to satisfy the Lawson criterion.

10.2.1.1 Pinches and Pulsed Power

Inertial confinement research began with pinches. These are plasmas created with a pulsed current, whose B-field compresses the plasma to higher density until the plasma pressure is balanced by the magnetic field pressure. Figure 10.4 shows a simple z-pinch (zed-pinch in the U.K.), like the one described theoretically as early as 1934 by W.H. Bennett. This type of pinch suffers from two instabilities: a sausage instability, shown in Fig. 10.5, and a kink instability, shown in Fig. 10.6. In the sausage instability, if a bulge develops in a linear pinch, the B-field is weakened with the new field lines. The plasma pressure is then able to push the lines further out. The opposite case of a reduced radius neck developing in the plasma is shown in Fig. 10.5. In the kink instability (Fig. 10.6), a kink, or bend, in the plasma will cause the B-field to be stronger on the inside of the curve than on the outside, and the magnetic pressure difference will enhance the kink. By adding a DC magnetic field to the pinch, these instabilities can be slowed down, but such pinches could not achieve confinement times adequate for fusion.

In 1952 James Tuck at Los Alamos in the U.S. made a toroidal z-pinch called the Perhapsatron. To drive the current, the plasma was threaded through an iron core and was the secondary winding of a transformer. This was one of the first toroidal experiments. In the U.K., a large toroidal "zed-pinch" called Zeta was built and exhibited at the 1958 Geneva conference, at which each nation showed what it had been doing while fusion was a classified subject. Neutrons were observed from Zeta which indicated that it had produced fusion reactions. However, the DT reactions were found to come from collisions on the wall, not the interior, much to the chagrin of my good friend Peter Thonemann.

Z-pinch. The z-pinch is so simple that it was not easy to give up on them in spite of their unstable nature. One solution was to drive a current through an array of hundreds of fine metal wires, as was done by T.W.L. Sanford et al. in 1995. Results from these and later wire array experiments are discussed in the context of a series

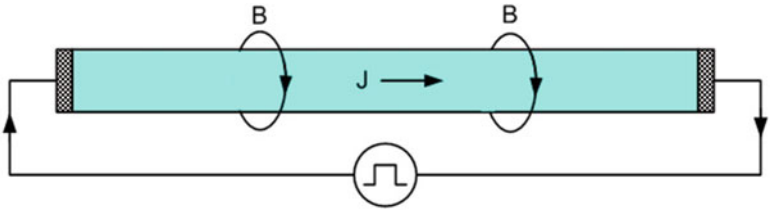

Fig. 10.4 A Z-pinch, or Bennett pinch

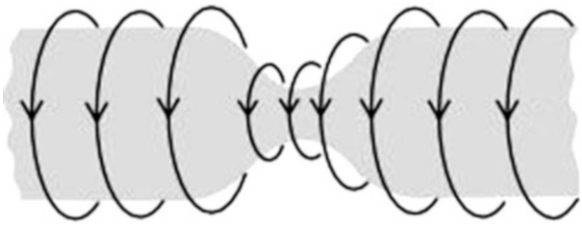

Fig. 10.5 Mechanism of a sausage instability

Fig. 10.6 Mechanism of a kink instability

of distinct physical mechanisms by Malcolm Haines *et al*. in 2005. The wires not only provided a hard core for the pinches, but they also stabilized the kinking in neighboring wires. Rayleigh–Taylor instabilities then made regular indentations along the linear plasmas. Related experiments were done with imploding cylindrical liners. Though the main purpose of these experiments was to create X-rays, a capsule containing deuterium, struck by such implosions, could produce 10^{10} DD fusion neutrons. A very large experiment, the Z-machine, at Sandia in New Mexico in the U.S., focused a number of these pinches onto a small wire-array target enclosing a DD-filled capsule inside a *hohlraum* (defined later) to produce fusion.

The power to the pinches was delivered through thick coaxial "cables" which used demineralized (high resistivity) water as a dielectric between metal cylinders. Water has a high dielectric constant of 80. The power was stored in compact megajoule capacitor banks. The capacitors are charged in parallel, slowly, and discharged in series, fast, in order to pulse-charge the water-dielectric coaxial cables in under 1 μs. This process is shown in Fig. 10.7.

A spectacular discharge on the surface of the demineralized water tank in the Z-machine is shown in Fig. 10.8. Such discharges occur only at late time in normal operation and do not affect the electrical energy delivered to the load during the main power pulse.

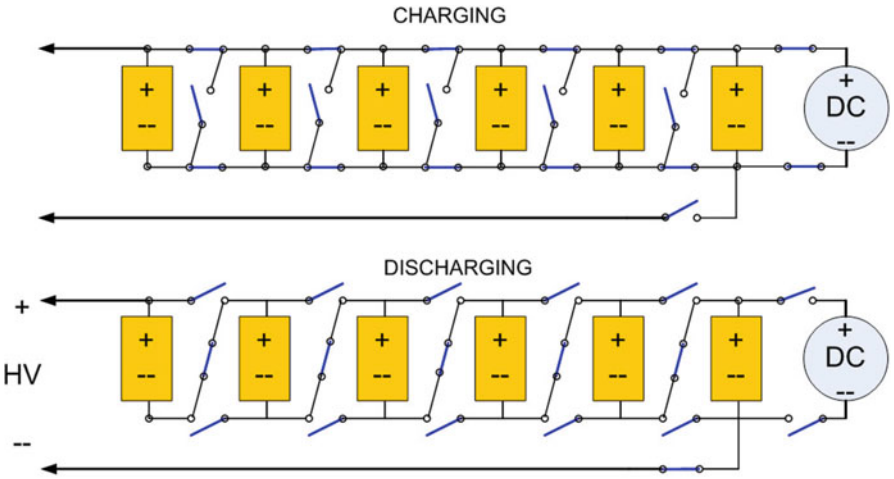

Fig. 10.7 Mechanism of charging and discharging a Marx bank

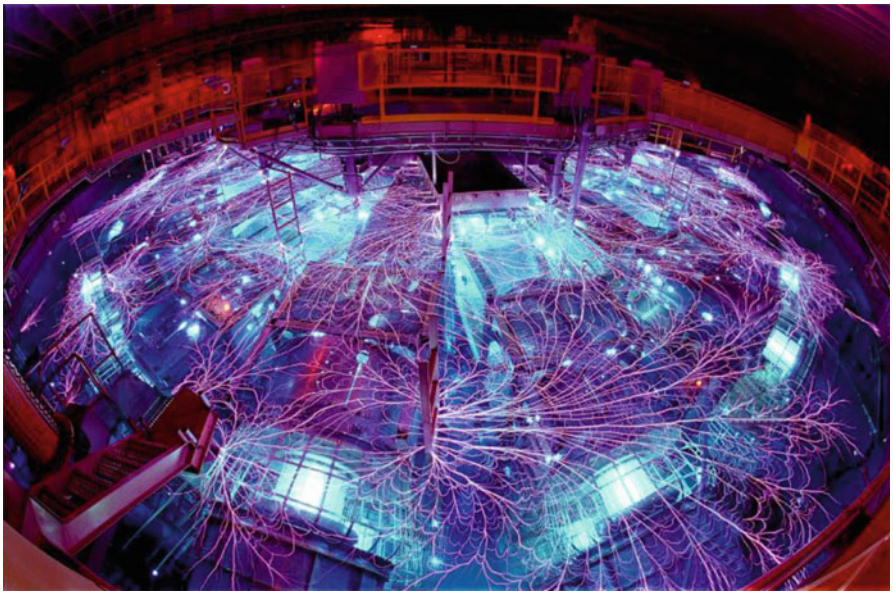

Fig. 10.8 The Z-machine at Sandia, NM

Smaller pulsed-power systems at universities can deliver ~1 TW of power in 100-ns pulses. A megajoule of energy is only the amount required to boil half a cup of water, but to deliver this energy in 100 ns takes a large machine. The Z-machine, along with high-power lasers, represent significant advances in technology, but they do not directly relate to fusion energy. Electric power must be steady and

continuously available, and this is difficult to supply with pulsed systems operating at less than 10 Hz. The largest pulsed plasma machines carry out experiments a few times a day at best.

The equilibrium condition of a simple z-pinch such as that in Fig. 10.4 is given by

$$\nabla p = \mathbf{J}\times\mathbf{B}, \tag{10.1}$$

where p is the plasma pressure, $\mathbf{B} = B_\theta\hat{\boldsymbol{\theta}}$, and $\mathbf{J} = J_z\hat{\mathbf{z}}$. By symmetry, derivatives in the $\hat{\theta}$ and $\hat{z}$ directions vanish. $\mathbf{J}$ is given by the time-independent fourth Maxwell equation

$$\mu_0\mathbf{J} = \nabla\times\mathbf{B} = \left(\frac{\partial B_\theta}{\partial r} + \frac{B_\theta}{r}\right)\hat{\mathbf{z}}, \tag{10.2}$$

So that

$$\begin{aligned}\mu_0\mathbf{J}\times\mathbf{B} &= (\nabla\times\mathbf{B})\times\mathbf{B} = (\nabla\times\mathbf{B})_z\hat{\mathbf{z}}\times B_\theta\hat{\boldsymbol{\theta}} \\ &= \left(\frac{dB_\theta}{dr} + \frac{B_\theta}{r}\right)B_\theta(-\hat{\mathbf{r}}) = -\left(\frac{1}{2}\frac{dB_\theta^2}{dr} + \frac{B_\theta^2}{r}\right)\hat{\mathbf{r}}\end{aligned}$$

The z-pinch equilibrium is thus given by

$$\frac{d}{dr}\left(p + \frac{B_\theta^2}{2\mu_0}\right) + \frac{B_\theta^2}{\mu_0 r} = 0. \tag{10.3}$$

Analogously, equilibrium of a θ-pinch is given by

$$\frac{d}{dr}\left(p + \frac{B_z^2}{2\mu_0}\right) = 0, \tag{10.4}$$

without the extra azimuthal term. This shows that the plasma pressure is balanced by the magnetic-field pressure.

Problem

10.1. A z-pinch of radius a has a uniform current $\mathbf{J} = J_z\hat{\mathbf{z}}$ and a plasma pressure $p(r)$ which is balanced by the $\mathbf{J}\times\mathbf{B}$ force. Derive the parabolic form of $p(r)$.

Theta pinch and reversed-field pinch. As shown in Fig. 10.9, a theta pinch has the plasma current going in the theta direction. After preionization, a pulse in the theta-pinch coils drives an azimuthal current $\mathbf{J}$, creating a plasma trapped in the B-field of the coils. By Newton's third law, this action creates a reaction: the current $\mathbf{J}$ is in the direction to produce a B-field on axis opposing the B-field of the coils. With sufficient current, the internal B-field can become larger than that from the coils, and we have a *reversed-field pinch*. The plasma can extend as far as the separatrix, which divides the internal field lines from those that extend beyond the coils.

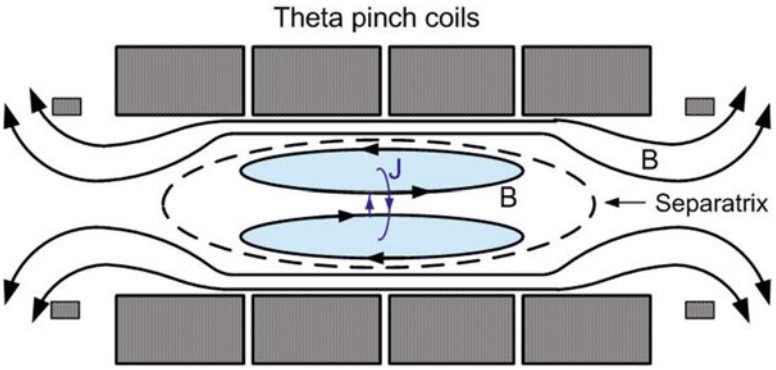

Fig. 10.9 Schematic of a reversed-field pinch (RFP)

The plasma is kept from sliding axially by the $J_\theta \times B_r$ force at its ends. At a critical current, the B-field on axis can be zero, and we have created a $\beta = \infty$ plasma!

The plasma in Fig. 10.9 suffers from instabilities. If the coils are long or far away, the plasma can tilt or slide in the horizontal direction. A hydromagnetic instability can occur at the ends because of the *unfavorable curvature* there. Though the pinch is necessarily pulsed, it lasts much longer than the instability growth time. The effect of curvature is illustrated in Fig. 10.10, where the animals represent plasma pressure from above. When the curvature is concave to the plasma, more plasma pressure can be supported, and *visa versa*. The curvature drift is described in Sect. 2.3.2 for a convex curvature. In Fig. 10.9, the sharp bends at the ends of the plasma are highly unstable, but fortunately the unstable fields (see Fig. 6.11) are short-circuited by the ions, which have large Larmor orbits and can cross the B-field. The finite-Larmor-radius effect was discussed in Sect. 2.4.

The Taylor state. Consider now a toroidal z-pinch such as the Zeta machine mentioned previously. The plasma is held in a toroidal B-field, and a current is driven through the plasma to produce a twist, turning the field lines into helices. It was found that, after a period of violent shaking, the plasma settled into a quiescent state. J.B. Taylor of the U.K. found that, if the helicity of the B-field is conserved, this relaxed state is a force-free, minimum energy equilibrium following the equation

$$\nabla \times \mathbf{B} = \lambda \mathbf{B}, \tag{10.5}$$

where λ is a constant. The long derivation is omitted here, but Eq. (10.5) is an equation that occurs often in different fields of physics.

10.2.1.2 Magnetic Mirrors

It is possible to trap charged particles between magnetic mirrors, which reflect particles with finite velocity $v_\perp$ perpendicular **B**. In Eq. (2.46) it was shown that the

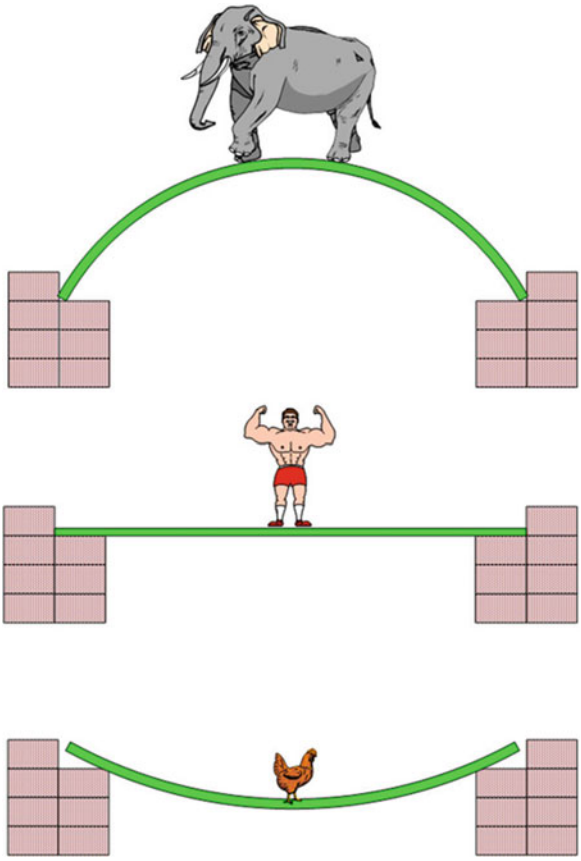

Fig. 10.10 The effect of curvature

magnetic moment $\mu = \frac{1}{2}mv_\perp^2/B$ of a particle is conserved. The energy W of a particle can then be written with constant μ:

$$W = \frac{1}{2}mv^2 = \frac{1}{2}mv_\parallel^2 + \frac{1}{2}mv_\perp^2 = \frac{1}{2}mv_\parallel^2 + \mu B.$$

Consider a barely trapped particle that is turned around at $B = B_{\max}$. Let $v_\parallel = v_\parallel$ at $B = B_0$ and $v_\parallel = 0$ at $B = B_{\max}$. Then we have

$$\begin{aligned} W &= \frac{1}{2}mv_\parallel^2 + \mu B_0 \quad \text{at} \quad B = 0 \\ W &= 0 + \mu B_{\max} \quad \text{at} \quad B = B_{\max} \end{aligned} \tag{10.6}$$

Since energy is conserved, this gives

$$\begin{aligned} 1 &= \frac{B_0}{B_{\max}} + \frac{\frac{1}{2}mv_\parallel^2}{\mu B_{\max}} = \frac{B_0}{B_{\max}}\left[1 + \frac{v_\parallel^2}{v_\perp^2}\right]_0, \\ R_m &\equiv \frac{B_{\max}}{B_0} = 1 + \frac{v_\parallel^2}{v_\perp^2} = \frac{v^2}{v_\perp^2}. \end{aligned} \tag{10.7}$$

R_m is called the *mirror ratio*, and particles starting with $v/v_\perp > \sqrt{R_m}$ are in the *loss cone* (Fig. 2.9) and are not confined by the mirror (Fig. 10.11).

The end losses from a simple mirror are so large that many modifications have been made to minimize these losses. Before we get to these, consider the stability of the plasma. At the center of the mirror, the field lines are convex to the plasma, and Rayleigh–Taylor instabilities can occur. At the throats of the mirror, the field lines are concave to the plasma, providing a stabilizing effect. If the machine is long enough to hold a useful volume of plasma, however, the unstable region dominates. One way to stabilize that part is to add "Ioffe bars", named after the inventor, which are four conductors carrying current in the axial direction, as shown in Fig. 10.12. The azimuthal fields from the bars, added to the mirror field, form twisted magnetic surfaces which have the minimum-B property. That is, the field strength |B| increases in every direction, forming a magnetic well for the plasma. This is a very stable arrangement, but the plasma still leaks out the ends of the mirror. In addition, mirrors suffer from another instability, the cyclotron-ion instability.

If one links the currents in the coils and the bars into a single conductor, a "baseball coil" is obtained, as shown in Fig. 10.13. A very large baseball-type magnetic mirror was built at Livermore Laboratory in the U.S. This heavy device (shown in

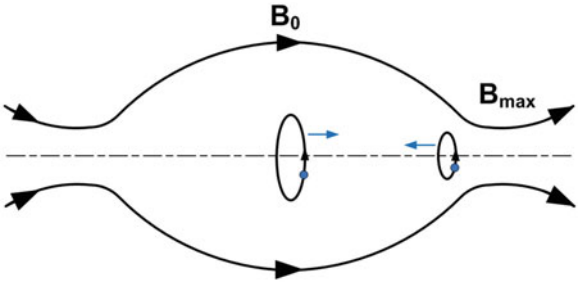

Fig. 10.11 Particle trapping by a magnetic mirror with $R_m \sim 4$

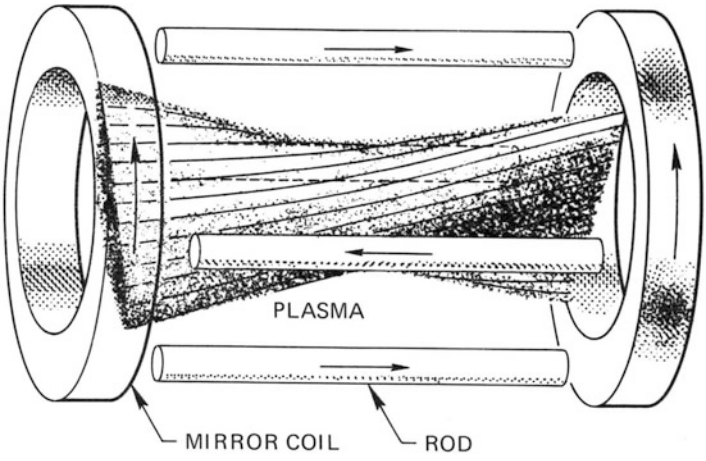

Fig. 10.12 A magnetic mirror with Ioffe bars

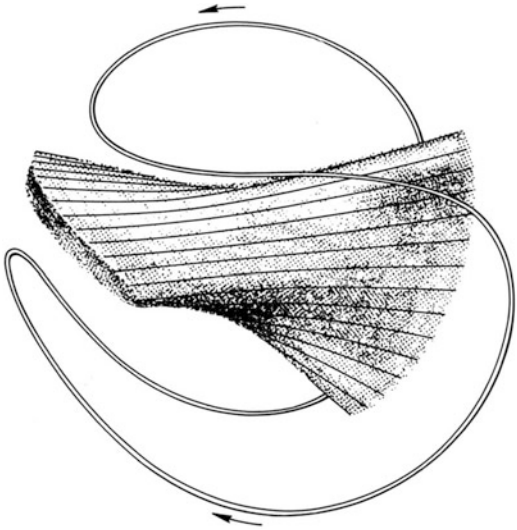

Fig. 10.13 Diagram of a baseball coil

Fig. 10.14 The MFTF-B mirror machine being moved by the old Roman method

Fig. 10.14, was being lifted into place when an earthquake struck, but what happened is inconsequential because the funding for mirror research was cut off at that time. The MFTF-B was never used and was turned into a walk-in museum for visitors.

Magnetic mirror research continued in Tsukuba, Japan, where a large axisymmetric mirror machine Gamma 10 was built (Fig. 10.15). This was a *tandem mirror*

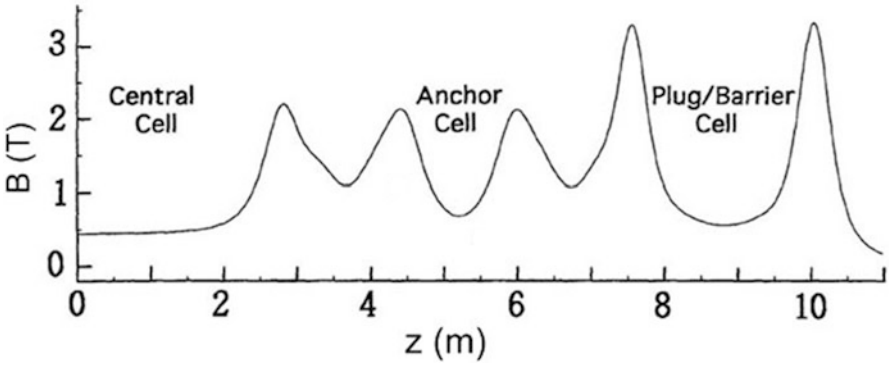

Fig. 10.15 Magnetic field configuration in a tandem mirror

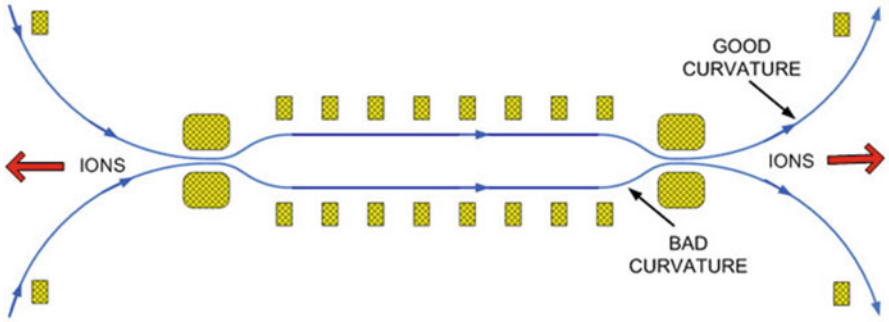

Fig. 10.16 Formation of an ion beam outside a simple mirror

consisting of several mirrors in series. For instance, one mirror could have minimum-B stabilization, while the end mirror could be a short one with a large mirror ratio for confinement. The main interest in mirrors was the possibility of direct conversion of plasma energy into electricity without going through a heat cycle. As ions collide, some will enter the loss cone and escape. These will be accelerated in the z direction because as B decreases, the conservation of μ means that $v_\perp$ will decrease, and hence $v_\parallel$ must increase. An ion beam will be ejected, as shown in Fig. 10.16, and it will be neutralized by electrons, which can escape easily by their frequent collisions. The ion beam will be sorted by energy and collected by a series of bins, as seen in Fig. 10.17, with the more energetic ones going farther before drifting sideways. Thus, the bins provide a DC current. Since the ions enter the bins at low energy, little heat is lost; and this would be an efficient way to convert fusion energy directly to electricity.

Mirrors are fueled by tangential injection of ions at the midplane. Mirrors are of course not immune to instability. In addition to the flute interchange instability in the central cell, there are instabilities driven by the anisotropy of the distribution functions, which have an empty loss cone. For instance, there is an Alfvén ion-cyclotron

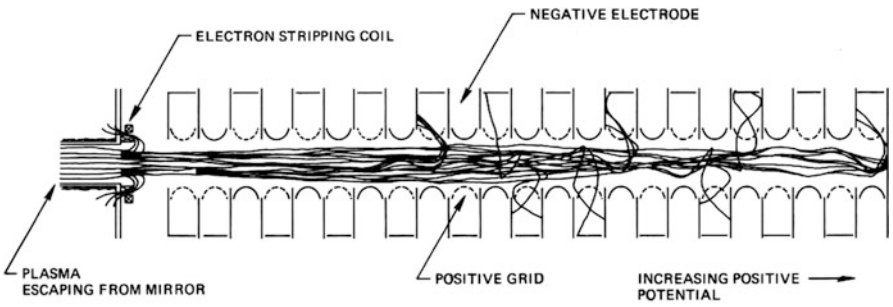

Fig. 10.17 Conceptual scheme for direct conversion of ion energy to electricity

instability. Compared with toroidal devices, mirrors do not confine plasmas as well and are not as suitable for fusion. However, they are useful for industrial applications where confinement is not as important as the ejected beams. They can also produce high-β plasmas for experiments not possible in low-β devices.

10.2.1.3 Reversed-Field Configurations

The possibility of creating a high-β plasma spawned a number of large experiments on reversed-field configurations (RFCs). An RFC is a high-β plasma requiring no toroidal field or conducting boundaries. A diagram of an RFC is shown in Fig. 10.18. Though the plasma is pulsed, many instabilities can grow faster than the pulse length. At the ends of the plasma is a region of bad curvature where gravitational instabilities are stabilized by finite ion Larmor radius r_{Li}. This is not simple, since r_{Li} varies rapidly in the nonuniform field. The most dangerous instability is thought to be the $n = 2$ tilt mode, shown in Fig. 10.19, where n is the azimuthal mode number. There is also an $n = 1$ rotational instability. Much of the work on FRCs is theoretical, but these instabilities have been observed. The plasma lasts microseconds, and the total temperature $KT_{\mathrm{e}} + KT_{\mathrm{i}}$ can reach 800 eV.

In the confined region of Fig. 10.18, plasma pressure is needed to balance the magnetic pressure. It can be shown that the average β is given by $\langle\beta\rangle = 1 - \frac{1}{2}(r_{\mathrm{s}}/r_{\mathrm{w}})^2$, where r_{w} is the wall radius. Since $r_s/r_w \leq 1$, $\langle\beta\rangle$ must be $>\frac{1}{2}$, and this is an intrinsically high-β device.

FRCs are translatable; that is, they can be pushed magnetically from one chamber to another. For fusion purposes, an FRC can, in principle, be translated into chamber with a DC magnetic field, a conducting wall for stabilization, and even "blankets" for capturing the neutrons and converting their energy into heat.

10.2.1.4 Stellarators

Confinement of plasma in a torus eliminates endlosses but introduces new problems. It is convenient to classify tori is by their aspect ratios. In a circular torus with

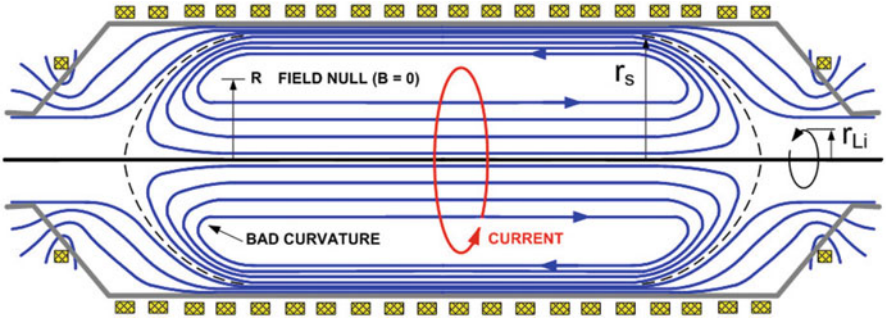

Fig. 10.18 Geometry of an RFC. The *dashed line* is the separatrix, with maximum radius r_s

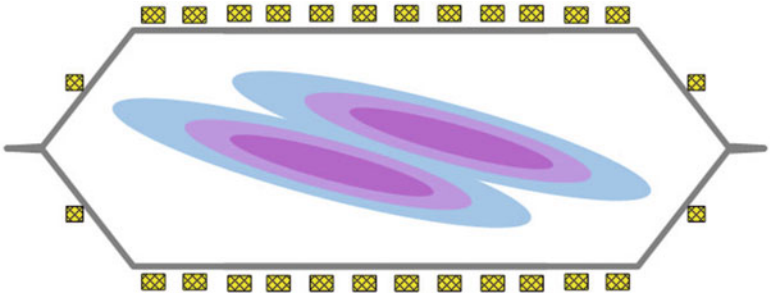

Fig. 10.19 Drawing of a tilt instability in an FRC

Fig. 10.20 A circular torus with aspect ratio R/a

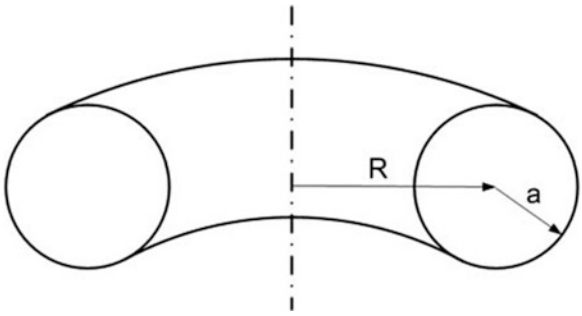

circular cross section, we can define R as the major radius and a as the minor radius, as shown in Fig. 10.20. The *aspect ratio* is defined as R/a. Proceeding from large to small aspect ratio, we start with stellarators.

Toroidal confinement began around 1951 when Lyman Spitzer, Jr., and Martin Schwarzschild built the figure-8 shaped Model A-1 machine at Princeton University. Being an astronomer, Spitzer named it a stellarator. The idea of a figure-8 came to Spitzer during a long ride on a ski lift at Garmisch-Partenkirchen. This was a solution to the problem of vertical drifts in a torus, as shown in Fig. 10.21. The

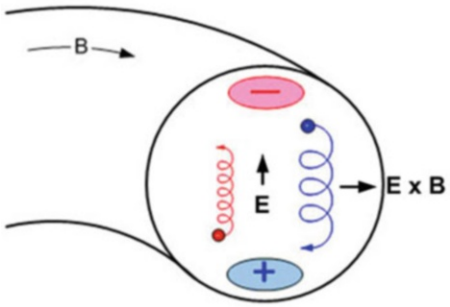

Fig. 10.21 Vertical drifts in a torus

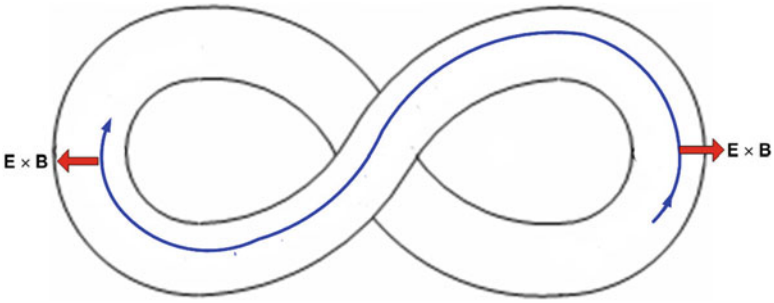

Fig. 10.22 Principle of a figure-8 stellarator

problem is this. In a torus **B** must be stronger on the inside (near the major axis, to the left here) than on the outside because the field lines are crowded together there. This causes the Larmor radii to be larger on one side of each orbit than on the other, giving rise to the grad-B drift [Eq. (2.24)], which depends on the sign of the charge. The electrons drift upwards, and the ions downwards, creating a vertical E-field. The resulting $\mathbf{E} \times \mathbf{B}$ drift is always outward, causing a loss of plasma.

To cancel this drift, one can twist the torus into a figure-8 shape, as shown in Fig. 10.22. As a particle follows a field line, its $\mathbf{E} \times \mathbf{B}$ drift is towards the outside in one half, and back towards the inside in the other half. A demonstration model of a figure-8 stellarator is shown in Fig. 10.23. This was built for the Atoms for Peace conference in Geneva in 1958, an event at which all nations revealed their secret work on fusion. An electron gun could be inserted into the model to accelerate electrons that traced out the field lines. An A-2 stellarator (fondly called the Etude) was operated by Kees Bol. The B-1 stellarator was run by the author in 1954, showing that electrons (not plasma) could be confined for millions of traverses around the 8, in spite of errors in the fabrication of the coils. A B-2 stellarator, shown in Fig. 10.24, was shipped to Geneva also, together with its power supplies and controls so that it could be operated normally. Meanwhile, T. Stix and R. Palladino at Princeton constructed a figure-8 stellarator in the form of a square, which they named B-64, or 8^2.

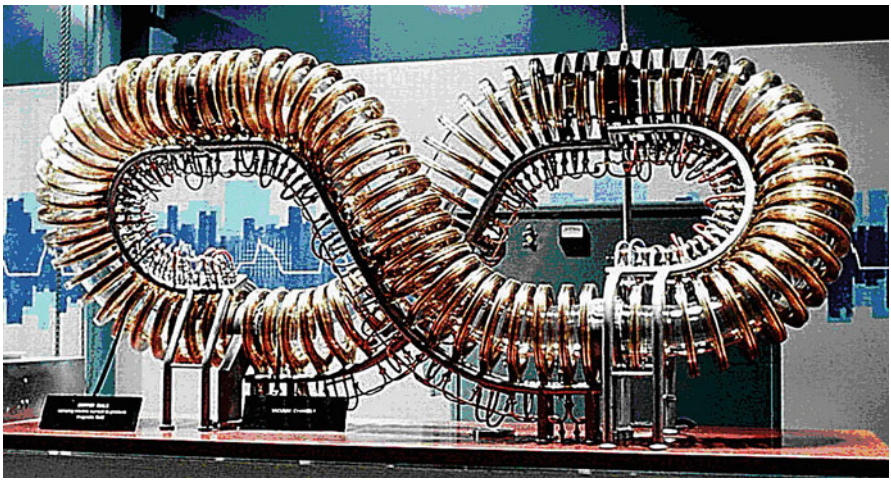

Fig. 10.23 Exhibit model of a figure-8 stellarator

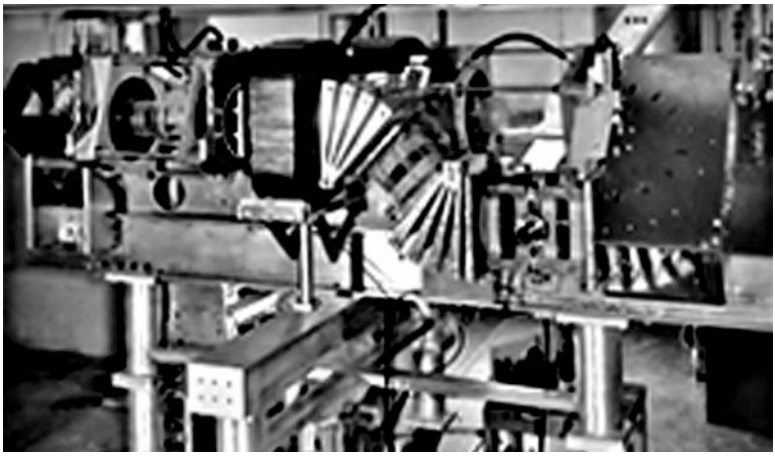

Fig. 10.24 The B-2 stellarator at Princeton

It was soon realized that the twist needed to cancel the vertical drifts could be produced without a figure-8 machine. What was needed was another set of coils wound helically around the torus, as shown in Fig. 10.25. This method had the additional advantage that the helical current could be varied. Th B-series of machines was replaced by the C-stellarator, a much larger machine with two important innovations: ion cyclotron heating, and divertors for capturing the escaping plasma. Previously, the plasma was heated only by ohmic heating, in which a current was induced around the torus by a transformer of which the plasma was the secondary winding. Since the plasma has a resistance caused by collisions of the

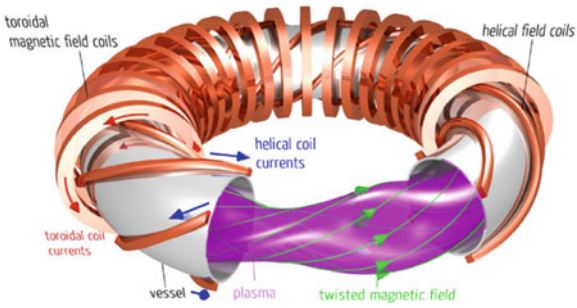

Fig. 10.25 A stellarator with helical windings [Google Images, 2015]

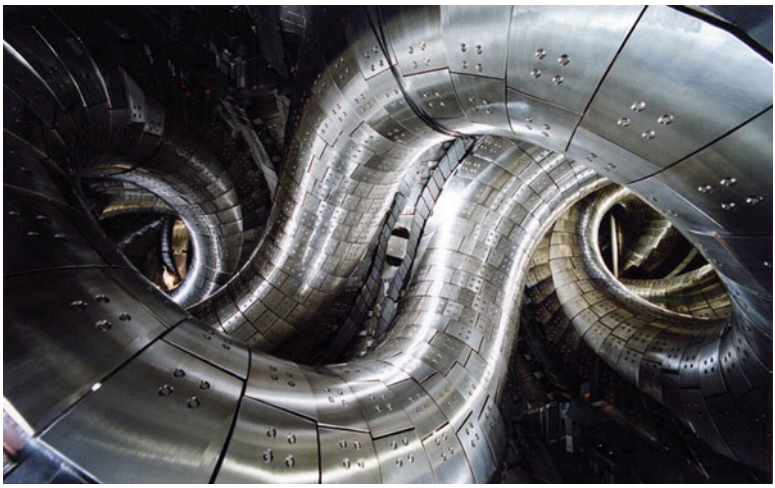

Fig. 10.26 The LHD stellarator in Japan [Google Images, 2015]

current-carrying electrons with ions, it was heated by the I^2R losses. The current created a poloidal B-field so that the field lines went through a poloidal angle ι (iota) each time they went around the torus the long way. A kink instability occurs when iota exceeds 2π. This is called the Kruskal-Shafranov limit. These difficulties have been overcome in tokamaks, which differ from stellarators in that the poloidal field is generated by the plasma current itself, and not by external coils. Modern stellarators use electron-cyclotron, lower-hybrid, and neutral-beam heating, as in tokamaks, and do not depend on ohmic heating.

Stellarators have been evolving since 1951, and variations with names such as torsatron, heliotron, heliac, and helias have been built in different countries. The most spectacular of these, the LHD (Large Helical Device) in Japan, is shown in Fig. 10.26. The entire vacuum chamber was shaped to follow the magnetic field. In Germany, D. Pfirsch and H. Schlüter combined the toroidal and helical coils into a series of 20 planar and 50 non-planar coils, several of each shape, to form the Wendelstein 7-X, shown in Fig. 10.27. This machine is under construction in

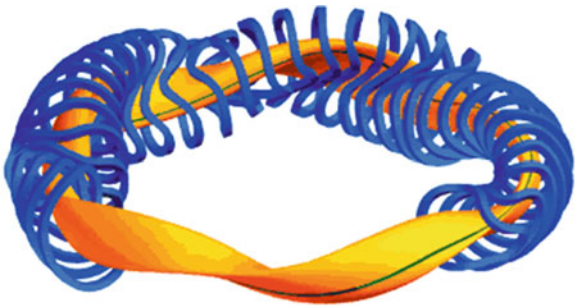

Fig. 10.27 Drawing of the Wendelstein 7-X stellarator [T. Klinger, Max-Planck Institute for Plasma Physics, Greifswald, Germany]

Greifswald, Germany. As with the LHD, the vacuum chamber is not round. To make room for all these coils, stellarators must have large aspect ratio.

With the large advances in the development and understanding of tokamaks, stellarators are no longer preferred for plasma confinement in fusion experiments. Nonetheless, stellarators have advantages which may make them more suitable than tokamaks for reactors. For instance, their poloidal field is created by helical windings and is not dependent on the plasma current, whose shape is not in direct control. Stellarators are also immune from "disruptions", which terminate tokamak plasmas unexpectedly and are not yet well understood.

10.2.1.5 Tokamaks

Invented in Russia, TOKAMAK is a Russian acronym for *toroidal chamber with an axial magnetic field*. Since tokamaks have become the favored form of toroidal fusion devices, so much is known about their behavior that only a few general characteristics can be given here. In tokamak literature, the rotational transform ι (iota) of stellarators is replaced by its reciprocal q. Thus, a field line that comes back to the same poloidal position after going around the torus twice the long way has $\iota = ½$ or $q = 2$. A typical q profile is shown in Fig. 10.28. The rational-q surfaces have field lines which close upon themselves and are special. The region $q < 1$ corresponds to $\iota > 1$ and is unstable. In tokamaks this instability has the form of sawtooth oscillations, as shown in Fig. 10.29 for T_i and $T_\mathbf{e}$ *vs*. time at $q = 1$. As the temperature rises at the center, the resistivity lowers, and the current density increases, thus driving the temperature higher until the configuration can no longer be sustained. Then the sawtooth crashes, ejecting a hot plasma outwards. Unlike stellarators, tokamaks have a self-organized plasma that generates its own behavior to achieve an equilibrium.

It is clear that the profile $q(r)$ should depend on the current profile $J(r)$. An example of this variation is shown in Fig. 10.30. It is seen that more peaked $J(r)$'s give higher $q(a)$'s. The particles, both ions and electrons, travel in interesting orbits on these magnetic surfaces.

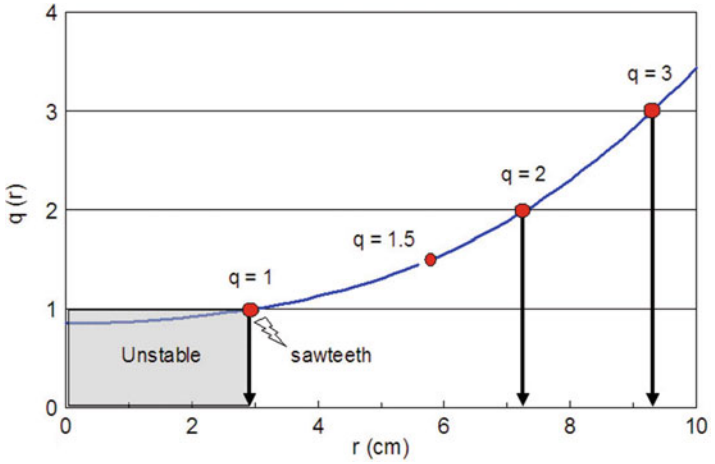

Fig. 10.28 A typical q profile in a tokamak

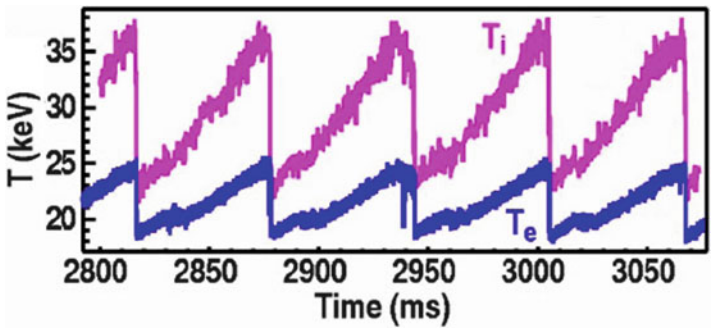

Fig. 10.29 Sawtooth oscillations in a tokamak

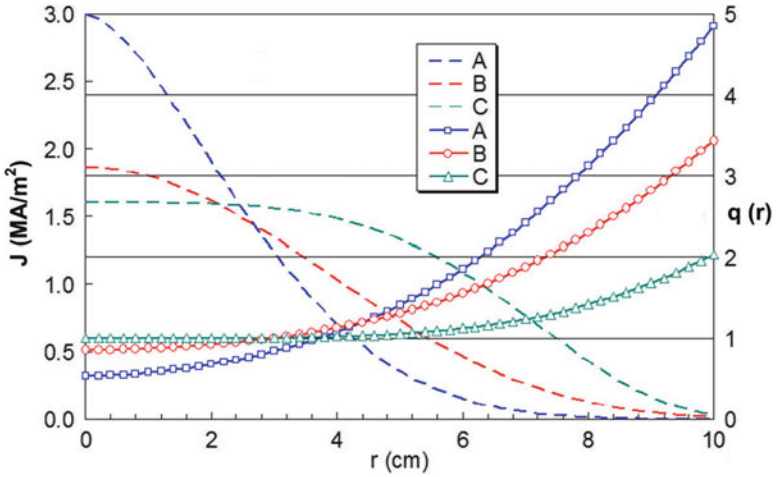

Fig. 10.30 The q profile for three different J profiles

Islands and Bananas

At the radii where q is a rational number, the field lines form magnetic islands. An example of this is shown in Fig. 10.31. In the islands, a particle will hop from one island to the next, eventually returning to the initial island in a different position. Its intersections with this cross section will trace out the islands. However, some particles can't go all the way around the torus. Consider the trajectory shown in Fig. 10.32. Since the B-field is stronger on the inside of the torus (nearer the major axis) than on the outside, a particle with small $v_{\|}$ can be mirror-trapped and reflected back. Projected onto a cross-sectional plane, this orbit resembles that in Fig. 10.33 and is appropriately called a *banana* orbit. These orbits can cause enhanced diffusion

Fig. 10.31 Magnetic islands at the $q = 3/2$ surface

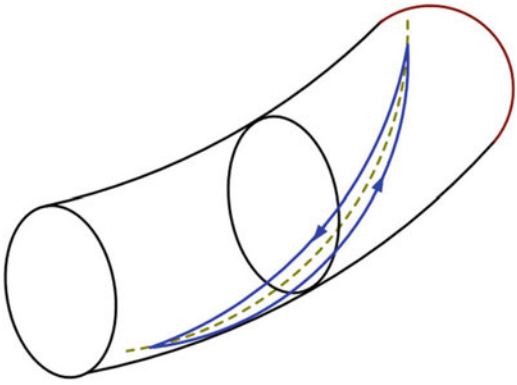

Fig. 10.32 Mirror-trapping of a particle in a torus

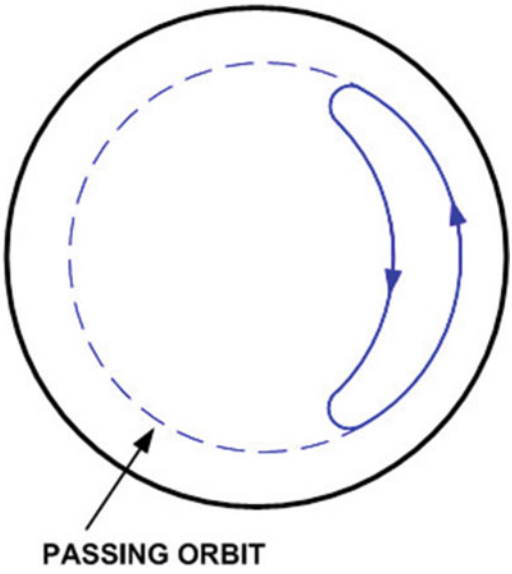

Fig. 10.33 A banana orbit. A particle with larger $v_{\parallel}/v_{\perp}$ would follow the dashed orbit

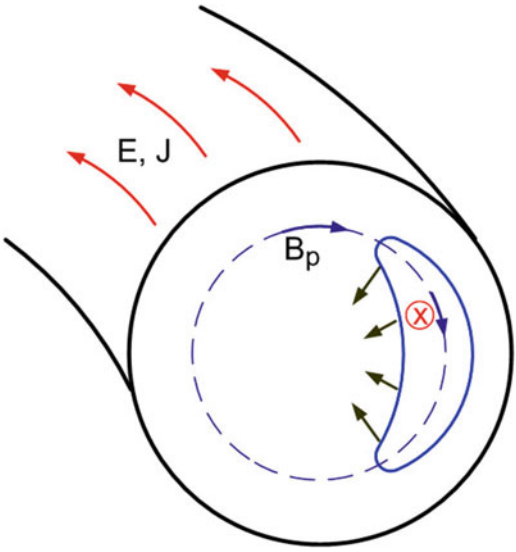

Fig. 10.34 Mechanism of the Ware Pinch

of plasma. Normally, a collision can result in a random-walk step the size of a Larmor diameter (Fig. 5.17); but now a particle can jump from one banana to another. The result is that diffusion depends no longer on the toroidal field B_{ϕ}, but on the weaker poloidal field B_{θ}. These effects contribute to "neoclassical diffusion" (see Fig. 5.22).

An effect associated with bananas is the Ware Pinch, illustrated in Fig. 10.34. Particles in banana orbits have an $\mathbf{E}_{\phi} \times \mathbf{B}_{\mathbf{p}}$ drift which is always inward, just as in a

linear z-pinch. Thus, bananas tend to move inward, countering collisional diffusion outward. The inward velocity of a Ware pinch is given by

$$v_{Ware} = (2 \pm 0.5) A^{-1/2} E_\phi / B_\theta, \tag{10.8}$$

where A is the aspect ratio, and the range covers details such as Z_{eff}.

Bootstrap Current

Another interesting effect in tokamaks is the *bootstrap current*, a current that arises, enhancing the toroidal current, as the plasma diffuses outward, as if the tokamak is pulling itself up "by its own bootstraps". This expression, originated around 1781, means to overcome an impediment without outside help. Figure 10.35a is a reminder of Eq. (2.17) showing the velocity of its guiding center when a particle is pushed by a force perpendicular to **B**:

$$\mathbf{v}_f = \frac{1}{q} \frac{\mathbf{F} \times \mathbf{B}}{B^2}. \tag{10.9}$$

In Fig. 10.35b, the black arrows show the outward pressure force on the plasma in a monotonic density profile. This causes the azimuthal drift of electrons, which is innocuous. The toroidal current generates an azimuthal $\mathbf{B_p}$ (blue arrows). The electrons drift in *this* field $\mathbf{B_p}$, driven by ∇p, is the bootstrap current. It is always in the same direction as the main current and hence adds it. The bootstrap current can be as large as 70–90 % of the total current, and the tokamak is really pulling itself up by its own bootstraps.

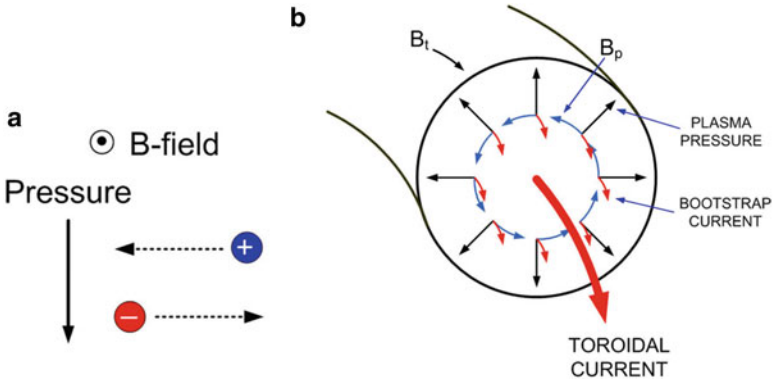

Fig. 10.35 Origin of the bootstrap current [the small *red arrows* pointing out of the paper in (**b**)]

The H-Mode

In 1982, Friedrich (Fritz) Wagner was heating the ASDEX tokamak with neutral beams when, at a certain threshold power, the plasma density suddenly doubled, and instabilities quieted down. This is now called the H (high)-mode. The density and temperature of the plasma did not fall to near zero at the edge but stopped falling at a pedestal level (Fig. 10.36a) as if there were a transport barrier there (Fig. 10.36b). Later experiments showed that there is a highly sheared azimuthal flow at the barrier which prevented normal outward diffusion of plasma. The plasma was instead lost in bursts called ELMs (Edge Localized Modes), a name which suggests that these were not well understood. The H-mode density is a factor 2–3 above previous values, now called the L (low)-mode. Other large tokamaks have also produced the H-mode, and now they all operate with it.

ELMs are thought to be "peeling-ballooning" modes driven by the large bootstrap current caused by the sharp pressure gradient in the thin pedestal layer. Peeling is a form of the kink mode. Ballooning is a bubbling out of the plasma into a weaker field, where extrusion can grow more easily. The pedestal raises the β of the plasma, and thus the fusion power, which increases as β^2. The H-mode was an entirely unanticipated gift of nature. The conditions can be adjusted so that these large outward bursts of plasma are replaced by a stream of small bursts, called grassy ELMs. Even better, it is possible eliminate ELMs altogether. This has been achieved in the ASDEX Upgrade in Germany and the DIII-D in the U.S. with neutral beams counter-injected relative to the plasma current. Figure 10.37 shows the ELM activity as seen by the oscillations in the deuterium α-line D_α. As the power is raised, the tokamak goes from the L-mode into the H-mode. At first, there are ELMs, but a long period ELM-free H-mode ensues. The average density, however, is low in the ELM-free mode, as seen in Fig. 10.38. Apparently, the radial flux at high density cannot be transported to the open field lines leading to the divertor without ELMs.

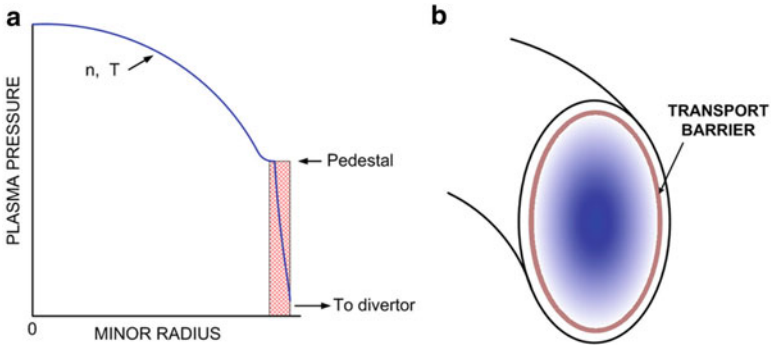

Fig. 10.36 The H-mode barrier

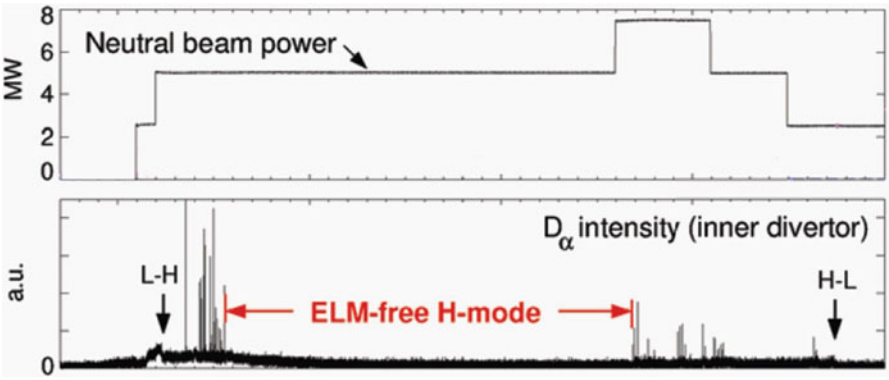

Fig. 10.37 An ELM-free discharge in ASDEX-U [Suttrop et al., Plasma Phys. Control. Fusion **45**, 1399 (2003)]

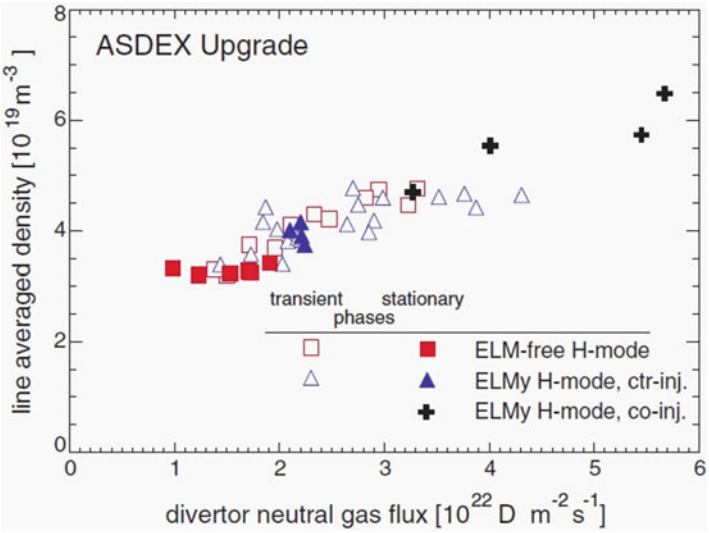

Fig. 10.38 Density increase from ELM-free to ELMy H-mode with counter- and co-injection in ASDEX-U [Suttrop et al., loc. cit.]

D-Shapes and Divertors

A toroidal plasma suffers from instabilities and other particle loss mechanisms that do not occur in cylinders. Since these effects are caused by the fact that one side of the plasma is closer to the major axis than the other, we can increase the volume of the plasma harmlessly by making the tokamak taller rather than wider. This has led to tokamaks with D-shaped cross sections, which are now commonly adopted. An example is shown in Fig. 10.39. At the top and bottom of the plasma there are "divertors", which capture the plasma exhaust. The confined part of the plasma is

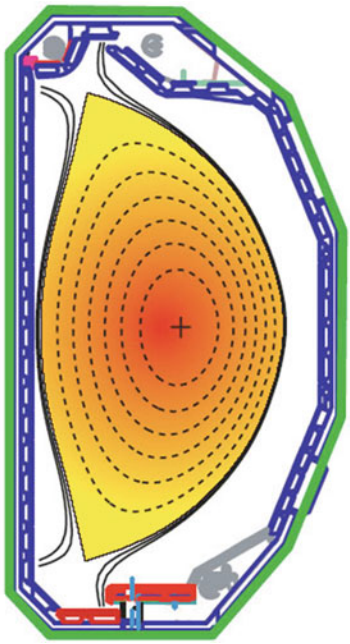

Fig. 10.39 Diagram of a D-shaped tokamak (from General Atomics, San Diego, California)

enclosed by the last closed flux surface, called the Scrape Off Layer. The surfaces outside of that capture the escaping plasma and lead it into the divertors, where high temperature materials and heavy cooling condense the hot plasma. Figure 10.40 shows the elongated chamber of the JET tokamak in England, which has been operating since 1983. Figure 10.41 shows a water-cooled divertor designed for a future tokamak.

The Density Limit

In assembling data from numerous tokamaks, M. Greenwald found that their average plasma density always fell below a hard limit which was proportional to the power input. This is shown in Fig. 10.42. It was thought that as the power was raised, the wall was bombarded by escaping ions, thus releasing high-Z impurities near the boundary. These would radiate and cool the plasma, increasing the resistivity there and thus changing the current profile into an unstable form. However, the density limit does not depend on the impurity level or the power. If the density is slowly raised in the H-mode until it reaches the limit, the H-mode disrupts unstably into the L-mode. If the density is allowed fall slowly, it decays at the rate that keeps the discharge at marginal stability. The density limit is not well understood.

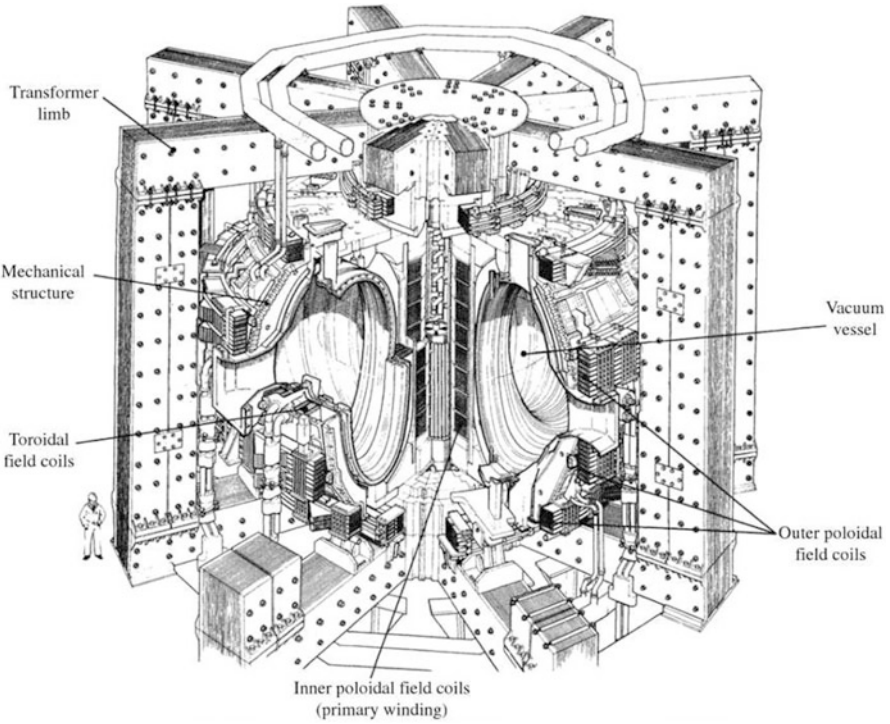

Fig. 10.40 Diagram of the JET tokamak in the U.K. [J. Wesson, *Tokamaks*, Oxford Science Publications (1987), p 658]

Fig. 10.41 Diagram of a divertor. CFC is a carbon fiber composite

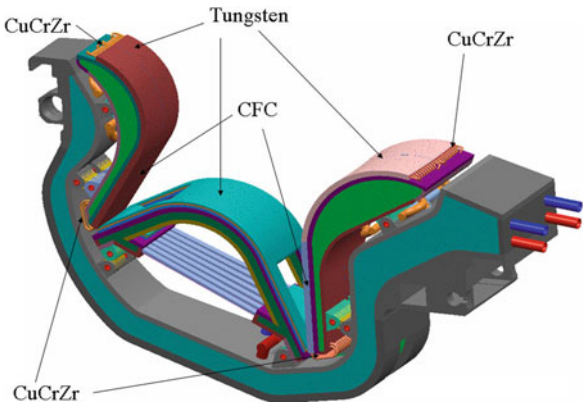

Heating and Current Drive

There are four main ways to heat a fusion plasma: ion-cyclotron resonance heating (ICRH). electron-cyclotron resonance heating (ECRH), lower-hybrid resonance

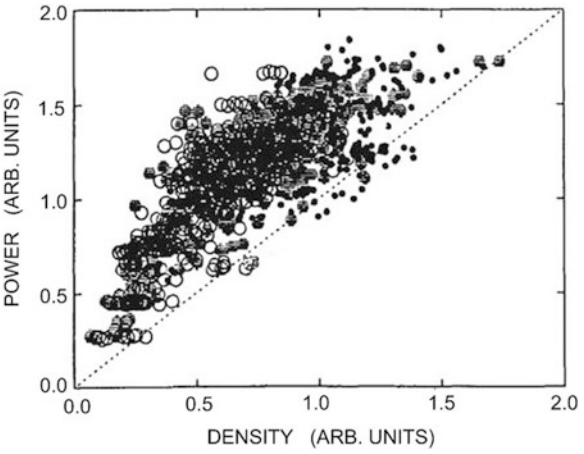

Fig. 10.42 The Greenwald density limit in tokamaks [M. Greenwald et al., Nucl. Fusion **28**, 2199 (1988)]

heating (LHRH), and neutral beam injection (NBI). In **ICRH** and **LHRH**, internal antennas are placed near the wall to excite ion cyclotron and lower hybrid waves, respectively. The wave energy is damped preferentially into ion energy. Though useful in experiments, such antennas would not survive in a reactor. These three waves are of quite disparate frequencies. For instance, at $B_0 = 3\text{T}$ and $n = 1 \times 10^{20}\ \text{m}^{-3}$, f_{ci} is 1.1 MHz, f_{LH} is 230 MHz, and f_{ce} is 84 GHz. ECRH, being in the microwave range, can be carried in waveguides and injected with a horn without requiring an internal antenna.

ECRH power, of order 100 GHz, is produced by gyrotrons, which produce electron cyclotron radiation by injecting an electron beam to gyrate in a strong magnetic field. A picture of a gyrotron is shown in Fig. 10.43. The magnet is at the bottom, and the top part collects the depleted beam. A bank of these, at 170 GHz and 1 MW, will be used in ITER. As shown in Problem 4.47, the cyclotron resonance can be reached only from the inside of the torus, where space in the central column is at a premium. For this reason, ECRH is often applied at $2\omega_{\text{c}}$.

Large tokamaks are mainly heated by the injection of neutral atoms (**NBI**) which can penetrate into the interior of the plasma before being ionized. These atoms must therefore have a large injection energy, typically hundreds of keV. For instance, the JT-60U tokamak in Japan has developed a 500-keV, 22-A ion source for an injector. To make a neutral beam one can start with a positive ion and add an electron, or start with a negative ion and strip an electron, which is easier. Neutral beam injectors typically start with negative deuterium ions (D^-), which are then passed through a gas such as lithium or cesium to be turned into neutrals. Neutral beams can be injected radially or, usually, tangentially in the same direction as the tokamak current.

Figure 10.44 shows the DIII-D tokamak at General Atomic in San Diego, California. The two large cylinders on the left are the neutral beam injectors. A beam dump on the far side captures the un-ionized beam. Neutral beam injectors tend to be larger than the tokamak itself and to dominate the laboratory. When

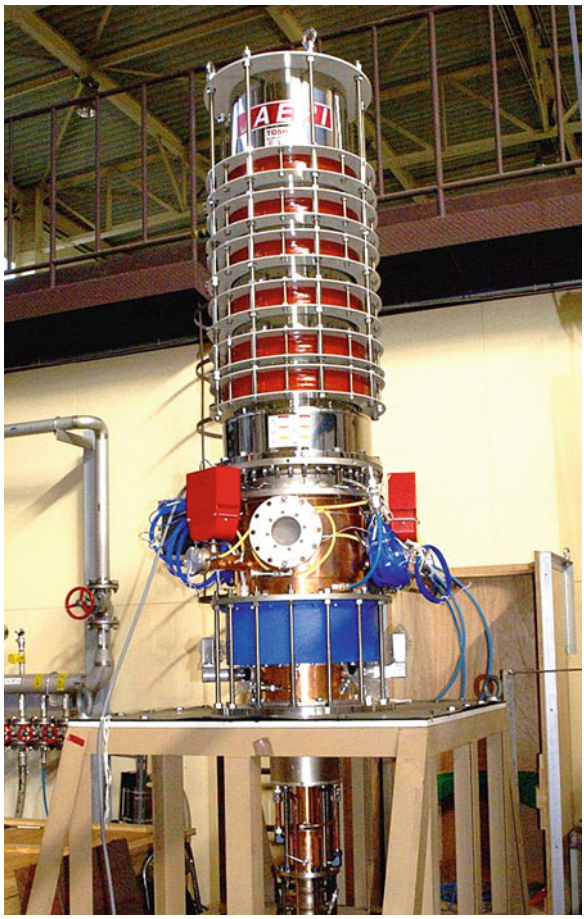

Fig. 10.43 A large gyrotron [ITER.org]

neutral beams are injected in the direction of the tokamak current, they contribute to that current when ionized. Varying the angle of injection affords a way to control the current profile. This is called non-inductive current drive, since it is steady-state and does not involve pulsing a transformer.

Electron cyclotron current drive is another way to achieve steady-state operation of a tokamak. To do this, waves at a frequency corresponding to ω_c somewhere in the interior of the plasma are injected from the inside of the torus. We can use Fig. 4.36 if we add a line representing the injected ω. If an X-wave is sent in from the outside of the torus, ω lies to the right, and the whole diagram moves to the right towards ω as ω_p increases. The wave will meet the cutoff at ω_R and be reflected. But if the wave is injected from inside the torus, where ω_c is larger than ω_L, it can travel to the radius where $\omega = \omega_c$ and give electron cyclotron current drive with its z component. The space in the central column very limited, and the need to inject from the inside is problematic.

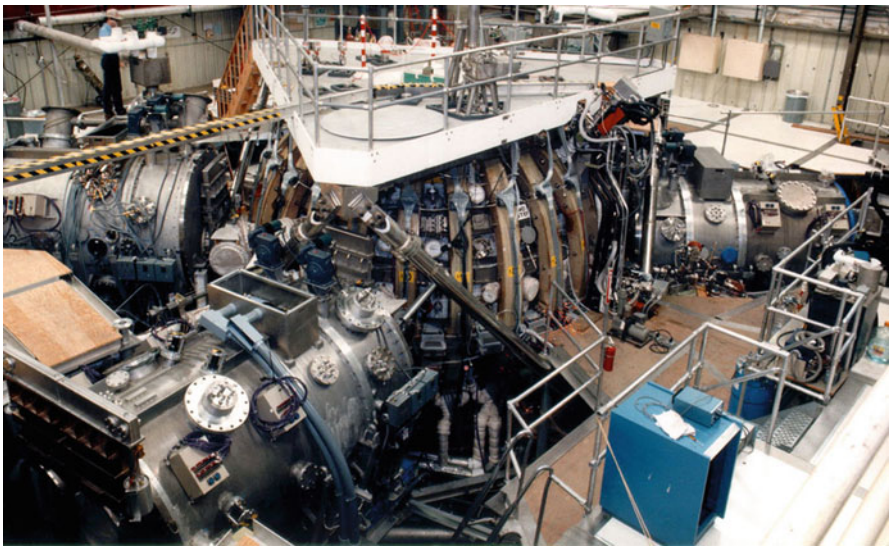

Fig. 10.44 The DIII-D tokamak in the U.S.

Disruptions

Tokamaks are subject to catastrophic events known as disruptions. There are many possible causes for this loss of confinement, but it is a global instability that causes a thermal quench—a sudden cooling of the plasma. The resistivity then increases, and the toroidal voltage can then accelerate electron runaways to MeVs. Large "halo" currents flow poloidally, partly in the plasma and partly in the wall. Large $\mathbf{J} \times \mathbf{B}$ forces are induced in the walls as $\mathbf{J}$ decreases. The D-shaped plasma "falls" vertically, as shown in Fig. 10.45. It is sometimes possible to anticipate a disruption when oscillations appear in Mirnov pickup coils near the edge. In that case, the disruption can be prevented by injection of a neutral gas such as He or Ne through a fast valve. It is clear that disruptions must be avoided in a reactor, and this can be done by operating the tokamak below its maximum power. With superconducting magnets, tokamaks can run almost steady state. The EAST (Experimental Advanced Superconducting Tokamak) in China can run pulses as long as 1000 s without disrupting.

10.2.1.6 Spheromaks and Spherical Tokamaks

When the aspect ratio of a tokamak is reduce to the order of unity, the machine becomes a spherical tokamak. If the central column is removed and the plasma is injected, it forms a self-organized structure called a spheromak. A smoke ring is an example of a self-organized structure. Instabilities, especially the kink instabilities, are suppressed at low aspect ratios, probably because of the short connection length between good and bad curvature regions.

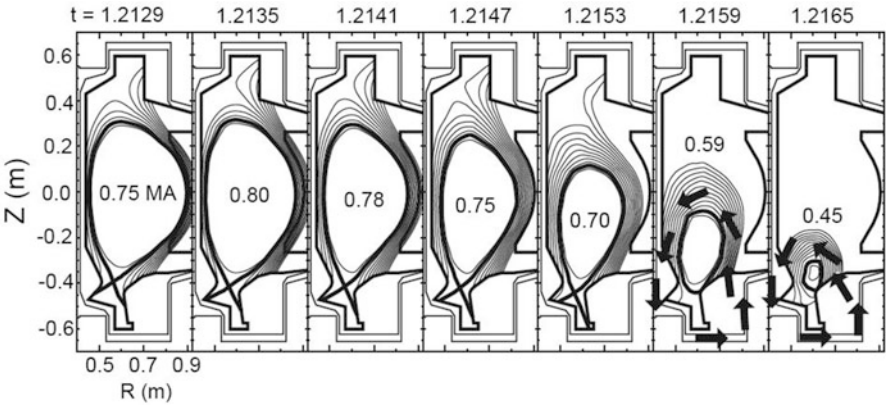

Fig. 10.45 Vertical motion of the plasma during a tokamak disruption [R. S. Granetz et al., Nucl. Fusion **36**, 545 (1996)]

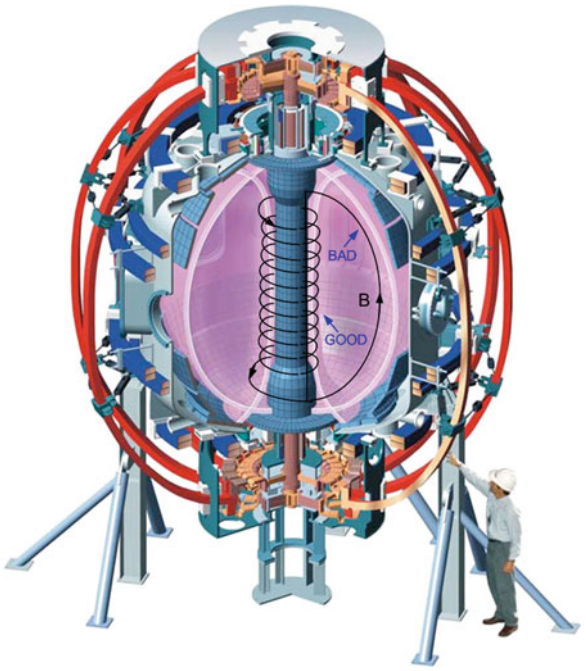

Fig. 10.46 Drawing of a spherical tokamak showing the regions of good and bad curvature of one field line [from F.F. Chen, *An Indispensable Truth* (Springer, 2011), p. 376; adapted from original by S. Prager, Univ. of Wisconsin]

A diagram of the NSTX spherical tokamak experiment at Princeton is shown in Fig. 10.46. A more compact machine, the MegAmpere Spherical Tokamak MAST is shown in Fig. 10.47. START (Small Tight Aspect Ratio Tokamak), a predecessor of MAST, achieved a beta of 40 %, an order of magnitude higher than the "Troyon limit" for ordinary tokamaks.

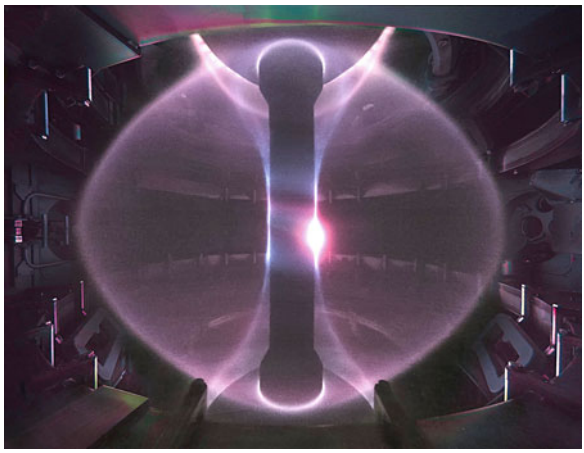

Fig. 10.47 The MAST spherical tokamak [Culham Centre for Fusion Energy, U.K.]

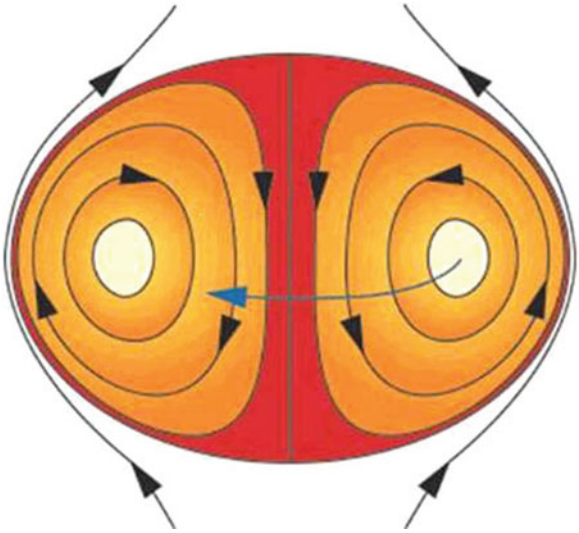

Fig. 10.48 Diagram of a spheromak [Univ. of Washington, College of Engineering]

A diagram of a spheromak is shown in Fig. 10.48. A toroidal current creates an entirely poloidal B-field, and there is no central core. This is formed by injecting a plasma with the right helicity into a flux conserver, as shown in Fig. 10.49.

10.3 Plasma Accelerators

In Fig. 7.17 we saw how a particle can be accelerated by a wave, thus causing damping of the wave. In 1979 John Dawson, in a paper with T. Tajima, proposed that this effect could be used to accelerate particles on purpose for experiments on

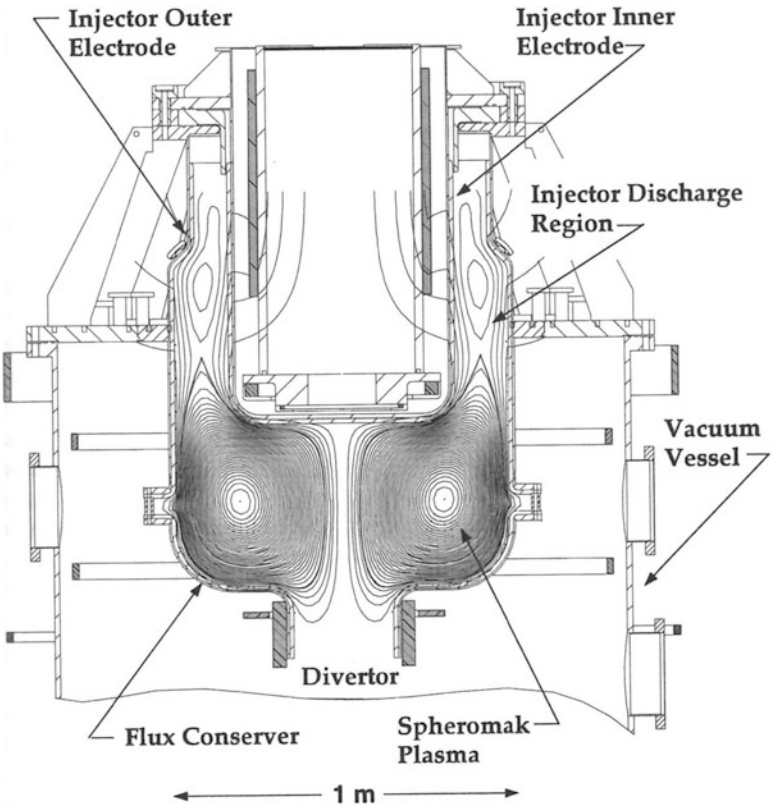

Fig. 10.49 Formation of a spheromak [E.B. Hooper et al., Lawrence Livermore National Laboratory Report UCRL-JC-132034]

nuclear physics and the structure of matter. Originally, Dawson envisioned accelerating particles traveling at an angle to a wave, as shown in Figs. 10.50, 10.51, thus gaining velocity faster than that of the wave. This idea spawned many experiments, principally in the U.S., Japan, and England, to develop a new type of accelerator. So far, only straight acceleration at zero angle has been tried.

There were two early ideas on plasma accelerators: *beatwave* and *wakefield*. In the beatwave case, two lines of a laser at $(\omega_0, \boldsymbol{k}_0)$ and $(\omega_2, \boldsymbol{k}_2)$ are set to resonate at ω_p, which is assumed to be much smaller than the laser frequencies. The beat frequencies are

$$\begin{aligned} \omega_1 &= \omega_0 - \omega_2 \equiv \Delta\omega \simeq \omega_p \\ k_1 &= k_0 - k_2 \equiv \Delta k \equiv k_p \end{aligned} \tag{10.10}$$

This excites a plasma wave with a phase velocity $v_\phi = \omega_1/k_1 \approx \omega_p/k_p$. Since plasma waves in a cold plasma do not depend on wavelength [Eq. (4.30)], k_p is allowed to

Fig. 10.50 Surfing at an angle to a wave [Google images]

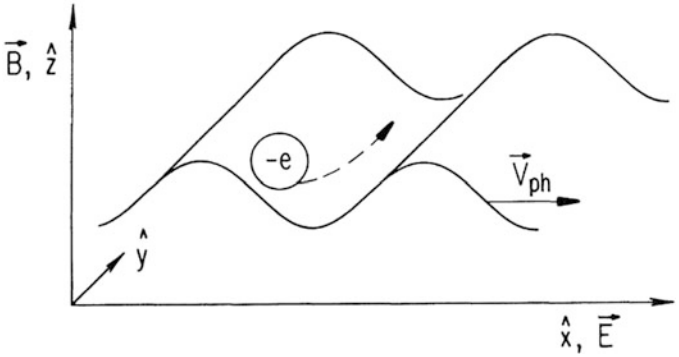

Fig. 10.51 Scheme of a surfatron accelerator [T. Katsouleas and J.M. Dawson, Phys. Rev. Lett. **51**, 392 (1983)]

have the above value. The phase and group velocities of the light waves are given by Eqs. (4.86) and (4.87), in which to subscript 0 pertains to the light waves. Thus

$$v_{\phi 0}^2 = \frac{\omega_0^2}{k_0^2} = c^2 + \frac{\omega_p^2}{k_0^2}, \quad v_{g0} = c^2/v_{\varphi 0} = c\left(1 + \omega_p^2/\omega_0^2\right)^{-1/2}, \tag{10.11}$$

and similarly for ω_2. In the usual limit $\omega_p \ll \omega_0$ so that $v_{g0} = d\omega_0/dk_0 \approx \Delta\omega/\Delta k$, we see from Eqs. (10.10 and 10.11) that v_{g0} of the light waves is nearly equal to the v_ϕ of the plasma wave. This assures that a laser pulse can continue to push particles trapped in the plasma wave over long distances.

At high plasma densities the assumption $\omega_p \ll \omega_0$ no longer holds true. The *critical density* n_c at which $\omega_p = \omega_0$ is defined by

$$\frac{n}{n_c} \equiv \frac{\omega_p^2}{\omega_0^2}. \tag{10.12}$$

The number n_c is a useful one in laser experiments. In terms of n_c, Eq. (10.11) can be written

$$v_\varphi \simeq v_{g0} = c(1 - n/n_c)^{1/2} \quad (n \ll n_c). \tag{10.13}$$

For example, $n_c \approx 1.0 \times 10^{25}/\text{m}^3$ for the 10.6-μm CO_2 laser line, $n_c \approx 1.21 \times 10^{25}/\text{m}^3$ for the 9.6-μm line, and $n_c \approx 1.29 \times 10^{25}/\text{m}^3$ for the 9.3-μm line. The beat frequency of 3×10^{12}/s between the 10.6- and 9.6-μm lines corresponds to the plasma frequency at $n = 1.1 \times 10^{23}/\text{m}^3$. This is a high density that can be produced by a pulsed plasma or even by the laser beams themselves. Beat waves were produced at UCLA in 1985, and acceleration of electrons by beat waves in 1993. Figure 10.52 shows two oscillations differing in frequency by 5 % and their beat wave, which has 20 times the wavelength, according to Eq. (10.10).

In wakefield acceleration, plasma waves are excited by a short pulse of electrons or photons. The waves have plasma frequency f_p and wavelength $\lambda \approx c/f_p$, since drive pulse travels at $v \approx c$. If the plasma wave has sufficient amplitude, electrons will be swept up by the wave and accelerated to $v \approx c$, gaining mass rather than velocity in the relativistic limit. It is also possible to inject electrons in the right phase by photoemission from a solid with a pulsed laser synchronized with the wave (Fig. 10.53).

The relativity factor γ of a plasma wave can be expressed simply in terms of ω_p:

$$\gamma \equiv \left(1 - v_\phi^2/c^2\right)^{-1/2} \tag{10.14}$$

Using Eqs. (10.12) and (10.13), we have

$$\gamma = [1 - (1 - n/n_c)]^{-1/2} = (n/n_c)^{-1/2} = \omega_0/\omega_p. \tag{10.15}$$

Real experiments involve beams, not the one-dimensional, infinite plane waves described so far. In two dimensions, one finds that in addition to regions of acceleration and deceleration, the wave has regions of focusing and defocusing. As computers advanced, it was possible to do cell-by-cell computer simulation to see the nonlinear development. One result is shown in Fig. 10.54. Here, a very short, intense laser or electron pulse is sent through a plasma. The ponderomotive force of the pulse ejects all the electrons, leaving a bubble of the slow-moving ions. As the pulse passes, the electrons are attracted back by the ion charge, forming a negative layer around the bubble and converging into an electron bunch behind the bubble.

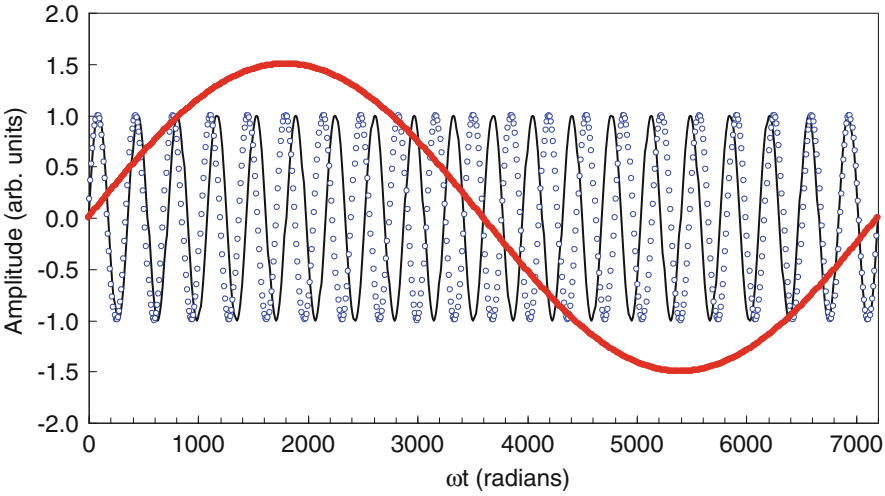

Fig. 10.52 The beat wave of two oscillations differing in frequency by 5 %

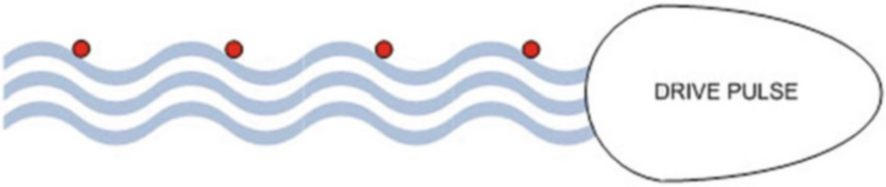

Fig. 10.53 Electrons surfing on the plasma wave behind a drive pulse

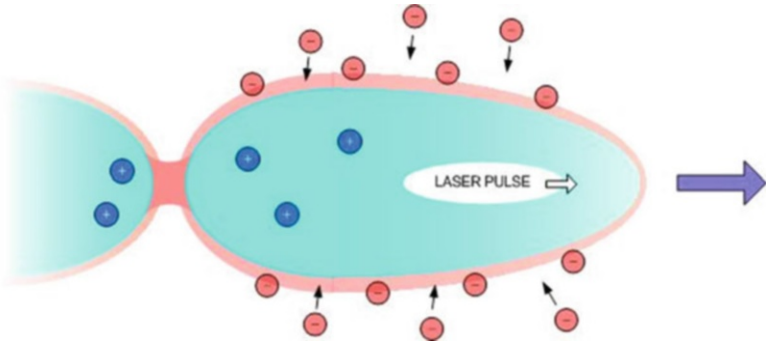

Fig. 10.54 A plasma bubble created by a short laser or electron pulse [adapted from Scientific American, February, 2006]

This has not been seen in experiment, but particle acceleration by the wakefield effect has been achieved in several countries with the world's largest lasers. The most successful of these experiments was done at the Stanford Linear Accelerator

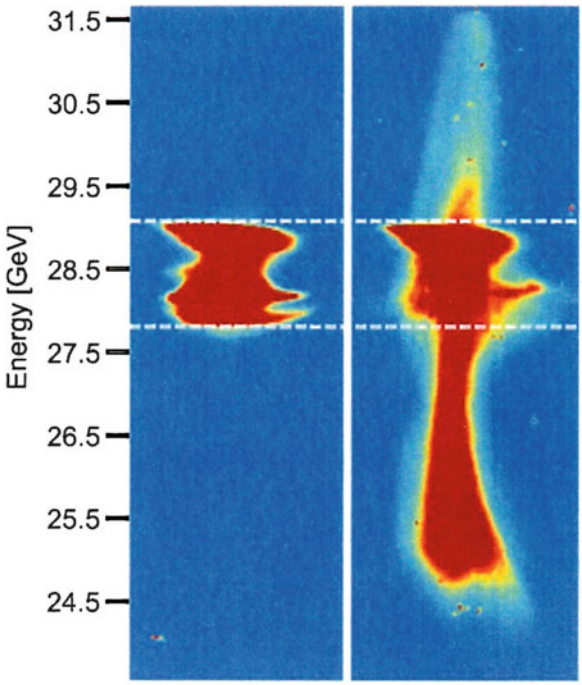

Fig. 10.55 Plot of energy vs. radius of an electron pulse in vacuum (*left*) and in a plasma (*right*) [M.J. Hogan et. al., Phys. Rev. Lett. **95**, 054802 (2005)]

Center (SLAC) by a team led by C. Joshi of UCLA. Figure 10.55 shows a highly relativistic 28.5-GeV electron pulse, 50 femtoseconds long, with 20 kA peak current. Electrons that have lost energy in forming the wake form the tail of the distribution, and the few electrons that have been accelerated to higher energy by the wake field are seen at the top. Note that this is not a spatial distribution, since all is traveling a the speed of light.

How large can the plasma wave (ω_p, $\boldsymbol{k}_\mathrm{p}$) get? Consider the linearized Poisson equation with stationary ions:

$$\begin{aligned} \varepsilon_0 \nabla^2 \phi = -k_p^2 \varepsilon_0 \phi = -e n_{e1} \equiv -en \\ e\phi = ne^2/\varepsilon_0 k_p^2 \end{aligned} \tag{10.16}$$

where $n \equiv n_{\mathrm{e}1}$ for this discussion. The maximum ϕ occurs when $n = n_0$, the background density. Hence,

$$e\phi_{\max} = \frac{n_0 e^2}{\varepsilon_0 m} \frac{m}{k_p^2} = \frac{\omega_p^2}{k_p^2} m \approx mc^2, \tag{10.17}$$

for highly relativistic waves. Let us define

$$\delta \equiv \phi/\phi_{\max} = n_1/n_0. \tag{10.18}$$

The magnitude of the plasma-wave E is then given by

$$|E| = |k_p \phi| = |k_p \phi_{\max} \delta| = \frac{\delta}{e} \frac{\omega_p^2}{k_p} m \simeq \frac{\delta}{e} \omega_p mc, \tag{10.19}$$

where, again, $\omega_p / k_p \approx c$. Extracting the n dependence, we have

$$|E| = \frac{\delta}{e} \omega_p mc = \frac{\delta}{e} \left(\frac{me^2}{\varepsilon_0} \right)^{1/2} n_0^{1/2} c = \delta \left(\frac{m}{\varepsilon_0} \right)^{1/2} n_0^{1/2} c = .096\, \delta\, n_0^{1/2}\, \mathrm{V/m}. \tag{10.20}$$

This is an extremely high field. For instance, if $n_0 = 10^{24}/\mathrm{m}^3$, E is of order 1 GeV/cm. In principle, this would allow linear accelerators to be shortened by three orders of magnitude.

Wakefield experiments in the 10's of GeV regime require a preformed plasma to prevent head-erosion of the laser pulse if it has to ionize the plasma also. Such a plasma has to have $n > 10^{16}$ cm^{-3} over $\geq$1 m and have a radius greater than the blow-out radius (Fig. 10.54) of order $c/\omega_p \simeq 17$ μm. Gases such as Li, Rb, or Cs can be used, but lithium has the advantage that it has a high second ionization potential of 75.6 eV, so that Li^{++} ions can be neglected. Typically, a plasma of density 5×10^{16} cm^{-3}, 1.5 m long, can be created with a 200 mJ laser pulse (4 TW for 50 fs). Such target plasmas were developed by K.A. Marsh and C. Clayton at UCLA for experiments at SLAC. Numerous variations of wakefield schemes have been developed with the aim of producing high quality electron beams with low emittance (transverse momentum). For instance, a low frequency laser, such as CO_2 can be used to form the wake, and a high frequency 800 nm laser used for injection of electrons. Finally, these methods can also be applied to positrons for electron-positron colliders.

10.3.1 Free-Electron Lasers

A related subject is that of the free-electron laser (FEL), which is the opposite of plasma accelerators in that an electron beam is used to create radiation rather than vice versa. A diagram of an FEL appears in Fig. 10.56. An array of permanent magnets, called a wiggler, is shown linearly, though it is usually helical. A relativistic electron beam is injected from the left and is wiggled by the Lorentz force from the magnets. It also creates a plasma and waves in the plasma. Without going into the mathematics, one can see that motion of the beam and the plasma can emit radiation, and when phased properly, this radiation can grow at the expense of beam energy. The depleted beam is caught in the beam dump at the right.

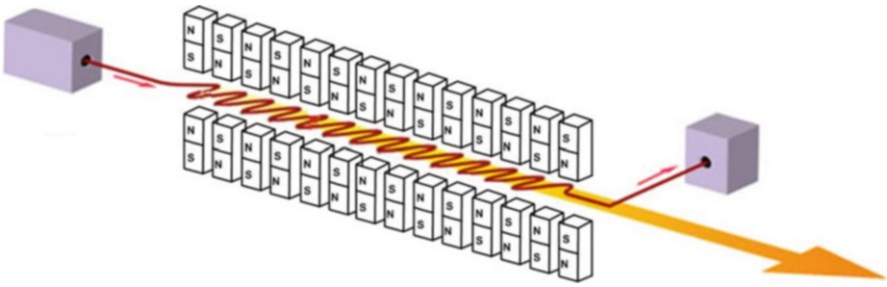

Fig. 10.56 Diagram of a free-electron laser (FEL)

10.4 Inertial Fusion

In the 1970s the advent of powerful lasers motivated physicists to explore the possibility of achieving fusion in short bursts rather than in a steady-state magnetized plasma. Among these were John Nuckolls and Ray Kidder at Livermore (now Lawrence Livermore National Laboratory); Keith Brueckner at University of California, San Diego; Keeve "Kip" Siegel in Michigan, and Chiyoe Yamanaka in Osaka, Japan. Siegel founded KMS Fusion but died in 1975 while testifying in Congress. Inertial fusion can also be achieved without lasers with collapsing magnetized metal "liners" in a z-pinch, or with ion beams, as in Fig. 10.8, but the greatest progress has been with lasers. The largest such experiment is the National Ignition Facility (NIF) at Livermore. This program could not have started without the LASNEX code written by Nuckolls, and laser fusion research still relies substantially on computer simulation.

10.4.1 Glass Lasers

In laser fusion, a fuel pellet is compressed by laser energy to a density $\rho \sim 1000$ times the density of solid DT (0.2 g/cm^3), or about 20 times that of lead, and temperature of order 10 keV. The Lawson criterion for breakeven in laser fusion works out to be

$$\rho r \geq 1\,\mathrm{g/cm^2}, \tag{10.21}$$

where r is the compressed radius. For $\rho = 200$ g/cm^3, r is ~50 μm.

There are two ways to achieve laser fusion. In *direct-drive* fusion, laser energy is directed as uniformly as possible over the surface of a fuel pellet, as shown in Fig. 10.57. The plastic ablator material is heated by the laser light and blasts off, pushing the layer of frozen DT to a density satisfying the Lawson criterion. To avoid Rayleigh–Taylor instabilities (Fig. 6.11), which would make small dimples

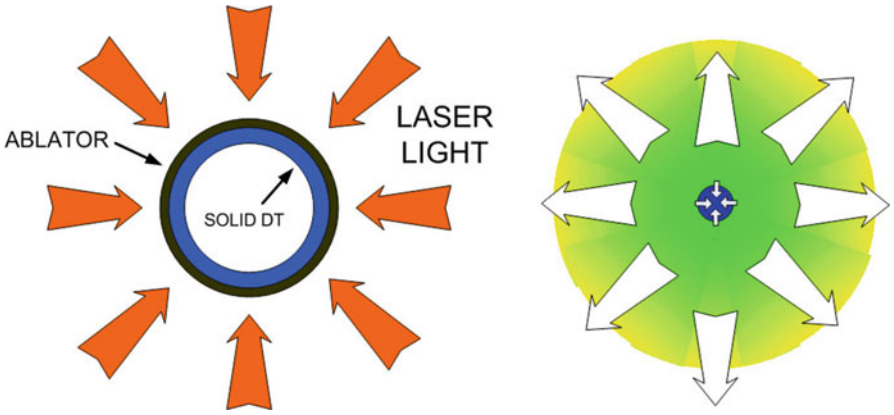

Fig. 10.57 Schematic of direct-drive laser fusion

grow into large gouges, the laser light is carefully smoothed out by random phase plates. The layer of frozen DT is serendipitously smoothed out by the small amount of heat from the slow decay of tritium into ^{3}He, an electron, and a neutrino. In the U.S., this approach is followed at the Laboratory for Laser Energetics in Rochester, NY.

In *indirect-drive* fusion, the capsule is compressed by X-rays inside a gold cylinder called a *hohlraum* ("empty space" in German). Figure 10.58 shows a hohlraum with laser beams entering holes at the ends. The beams must not hit the sides of the hole, or they would create plasma that will refract or reflect the beams. Once inside the hohlraum, the beams strike the walls, creating a bath of X-rays, which will then heat the capsule and compress it. This is a miniature version of an H-bomb. Several views of hohlraums are shown in Fig. 10.59.

In the U.S., indirect-drive fusion is explored at the NIF at Livermore. This facility is a marvel of engineering. Light from a single oscillator is preamplified and then split into 192 beams. The beams are amplified in Nd-glass plates lit by LED flashlamps powered by 422 MJ of capacitors. Faraday rotators and polarizers are inserted to prevent reflected light from being amplified backward and destroying the front end. Since parametric instabilities are less important at shorter wavelengths, the 1.05 μm Nd-YAG (neodymium-doped yttrium aluminum garnet) beams are frequency tripled by KDP (potassium dihydrogen phosphate) crystals to 351 nm in the green. A single dust particle on one of the glass plates will absorb enough laser light to damage the plate, which must be replaced. Refrigerator-sized replacement units are stored below beam lines and can be inserted into place. An early picture of the NIF laser bay is shown in Fig. 10.60.

The laser beams are mirrored in a switchyard to enter into a spherical target chamber, shown in Fig. 10.61. They must all reach the target within a few picoseconds. Light travels only 0.3 mm in a picosecond. Hence the lengths in this system the size of a football field have to be kept constant with temperature control.

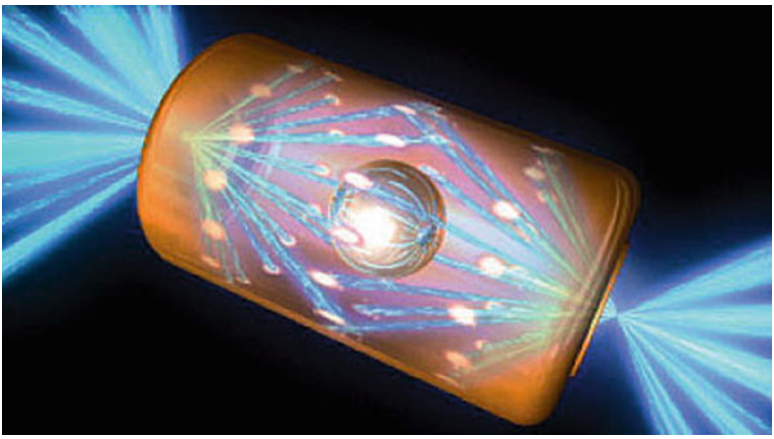

Fig. 10.58 Drawing of a hohlraum [courtesy of Lawrence Livermore Laboratory via Google Images]

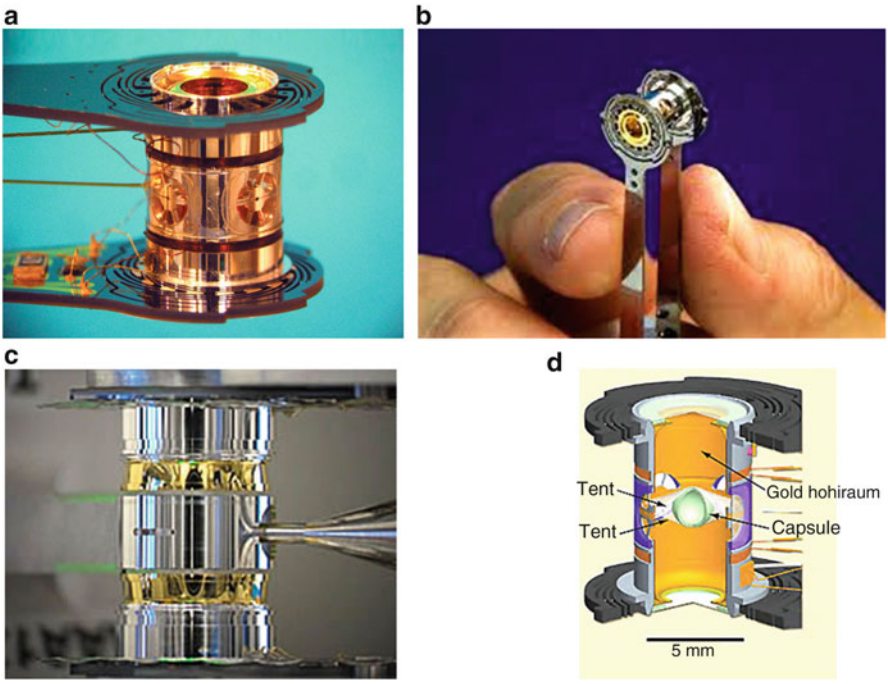

Fig. 10.59 Hohlraums: (**a**) a hohlraum in its holder; (**b**) size of a hohlraum; (**c**) a "rugby" hohlraum with an ellipsoidal cavity; (**d**) suspension of a capsule in a hohlraum with thin plastic membranes or "tents"

Fig. 10.60 The laser bay of the National Ignition Facility [courtesy of Lawrence Livermore Laboratory via Google Images]

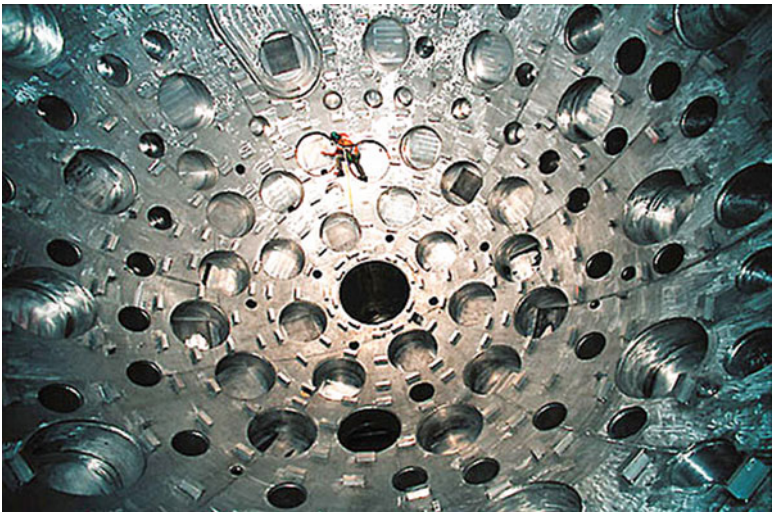

Fig. 10.61 The NIF target chamber, seen from inside [courtesy of Lawrence Livermore Laboratory via Google Images]. Note the figure of a man above center

The beams carry 15 MJ of 351 nm light, giving a peak power of 430 TW. The total electricity generation in the U.S. is about 0.5 TW on average.

Impressive as these numbers are, fusion with glass lasers is not an energy source. The goal of ignition, in which the alpha particles from the DT reaction keeps the plasma hot, has not been achieved. The most that has been achieved by 2015 is fuel gain, in which the fusion energy out is larger than the laser energy in, with a laser efficiency of about 1%. Furthermore, the NIF can pulse only twice a day to allow the glass to cool. A fusion reactor would require pulsing at 10 Hz. Each shot destroys a target such as that shown in Fig. 10.59. The hohlraum cannot simply be dropped from the top of the chamber; the DT ice would melt. The target has to be shot into the lasers' focus in exactly the right orientation. After each shot, the debris has to be cleared so as not to interfere with the next laser shot. Heavy products like gold take a long time to reach the wall. Liquid Li walls or FLiBe (fluorine, lithium, beryllium) waterfalls have been suggested to catch the gamma rays and other products but they cannot clear the whole volume rapidly. The NIF cannot lead to a fusion reactor. It is funded by the Nuclear Weapons Stockpile Stewardship program in addition to the Department of Energy and serves as a safe way to study such topics as the equation of state under extreme conditions without using underground nuclear explosions.

In addition to accurate focusing, the timing of the laser pulses is crucial. A simple intense laser pulse can drive the fuel into a center hotspot until the ρr criterion is exceeded, but one can do much better than that. Here are two ways. In *fast ignition*, the compression and heating phases follow each other, just as in a gasoline engine. First, one laser pulse compresses the fuel to the required density; then a second high-intensity, ultrashort pulse heats the core. The compression pulse can have less energy and uniformity than usual, so that the energy gain is 10–20 times higher than normal (Fig. 10.62).

In *shock ignition*, the general principle is to launch a series of shocks which overtake one another at the central spot. In NIF, this is done in just two steps with a single laser. Figure 10.63a shows the timing compared with that of a conventional single pulse. First, there is a low-velocity compression, which entrains more fuel mass and saves energy compared the normal procedure. This is followed by a strong

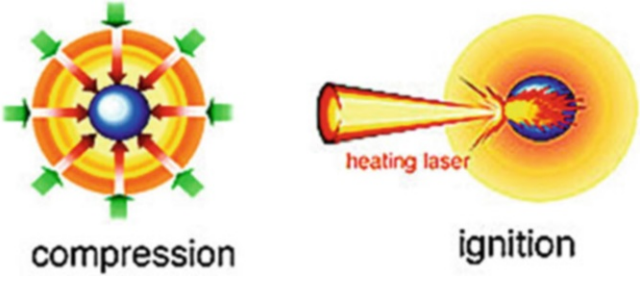

Fig. 10.62 Stages of fast ignition [modified from Google Images; originally from Los Alamos National Laboratory's *Dense Plasma Theory*]

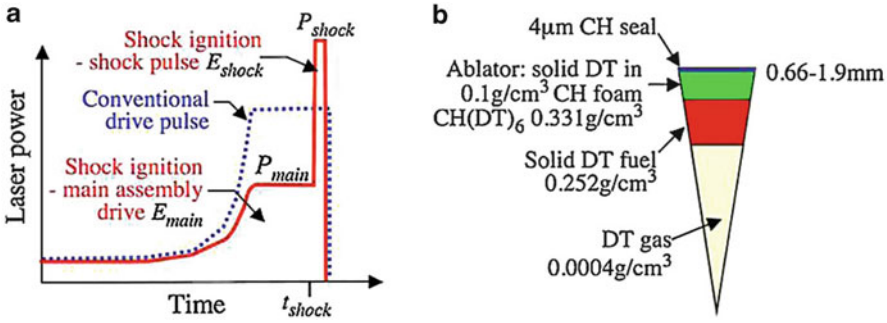

Fig. 10.63 (**a**) Time sequence of a shock ignition pulse, compared to a conventional pulse. The total time has to be short enough to avoid heating the hohlraum [L.J. Perkins et al., Phys. Rev. Lett. **103**, 045004 (2009)]. (**b**) Design of a capsule for shock ignition

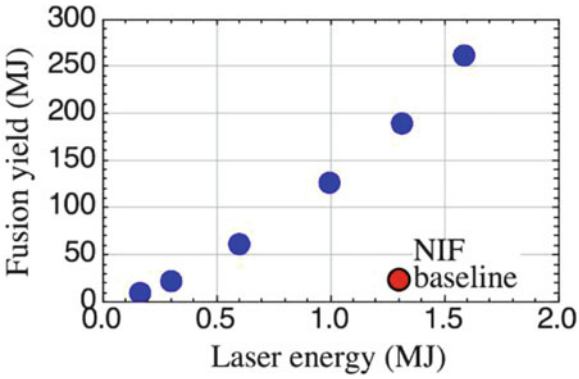

Fig. 10.64 Computed fusion energy from shock ignition compared with normal compression [L.J. Perkins et al., *loc. cit.*]

shock pulse timed to arrive when the compression reaches stagnation at a velocity of about 4×10^7 cm/s. The shock contains 20–30 % of the energy of the pulse. The hope is to generate 120–150 MJ of fusion power using only 1–1.6 MJ of laser power. Figure 10.63b is a possible design of a capsule suitable for shock ignition, and Fig. 10.64 shows the expected fusion energy *vs*. laser energy.

To improve the twice-a-day repetition rate, plans are to construct a High Repetition Rate Advanced Petawatt Laser System (HAPLS), designed in collaboration with the Czech Institute of Physics. The laser would produce 1 PW (10^{15} W) in 30 fs pulses at 10 Hz. In collaboration which Czech scientists, this would be installed at the Extreme Light Infrastructure Beamlines facility (ELI-Beamlines), under construction in Dolní Breźańy near Prague in the Czech Republic. Such high rep-rate lasers are already available in KrF (krypton-fluoride) lasers.

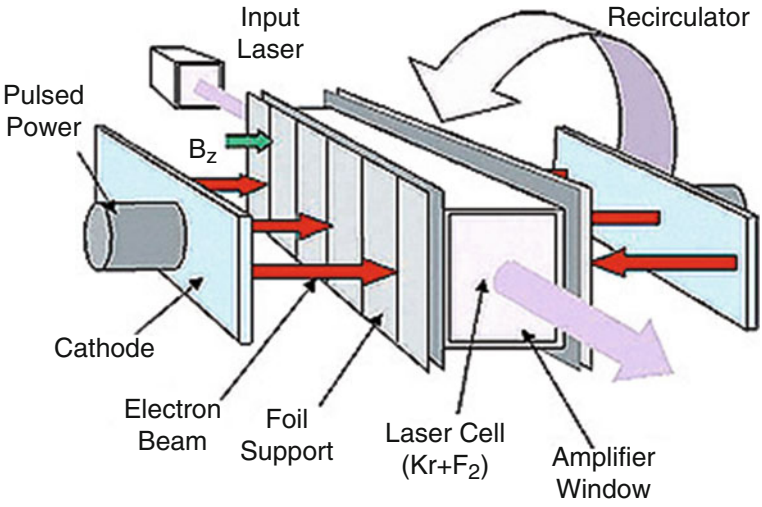

Fig. 10.65 Diagram of a krypton-fluoride laser amplifier [J.D. Sethian et al., Phys. Plasmas **10**, 2142 (2003)]

10.4.2 KrF Lasers

Krypton fluoride lasers, such as the Electra laser at the Naval Research Laboratory in the U.S., can pulse at 5 Hz at 400–700 J to give almost steady-state power. The technology can be extrapolated to 10^6 shots at 50–150 kJ for laser fusion. In the diagram of Fig. 10.65, an electron beam produced by pulsed power (Sect. 10.2.1.1) passes through a 1-mil (0.001 in.) Ti foil to ionize a cell containing Kr and F_2. The recirculator reflects the electrons to use them a second time. The KrF wavelength of 248 nm is even shorter than the 3ω, 351 nm wavelength of Nd-YAG lasers and is suitable for minimizing parametric instabilities. Though KrF lasers have much lower power than glass lasers, they can provide the rep rate needed for fusion.

10.5 Semiconductor Etching

All the computers, iPhones, iPads, and tablets are based on a semiconductor chip about 1 cm^2 in size and containing billions of transistors. The doubling of the transistor count every 2 years is known as Moore's Law, shown in Fig. 10.66. A "chip" can contain several cores, or Central Processing Units (CPUs). The progress is so rapid that in 1989 the largest Intel chip contained 1.18 million transistors with a critical dimension (CD) of 1 μm for its smallest feature. In 2014, the count increased to 5.56 *billion* transistors with a CD of 22 nm (0.022 μm).

Chips cannot be made without plasmas. The transistors lie on several layers, and connections are made between layers with copper or aluminum conductors

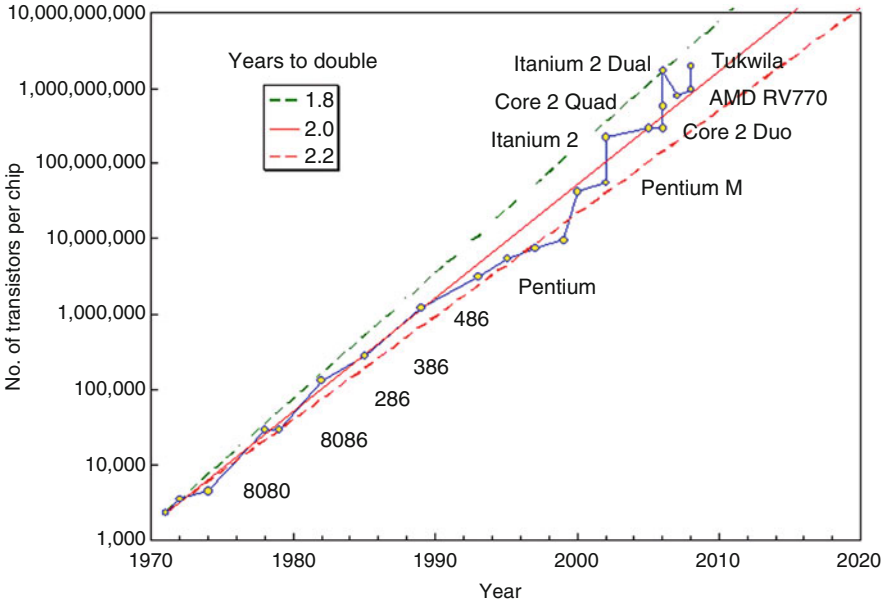

Fig. 10.66 Moore's law of transistors on a chip

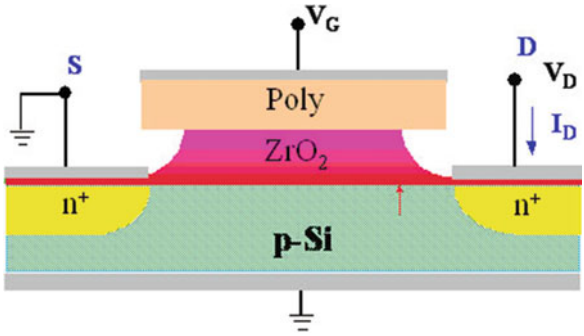

Fig. 10.67 Cross section of a transistor on a polycrystalline substrate

deposited into channels called *vias*. The transistors themselves are made by repeated plasma etching and deposition steps. Some transistors, called FinFETs, are themselves three-dimensional. Hundreds of chips are made at once on a 300-mm wafer of single-crystal silicon. The plasma must be uniform over the wafer. Chips near the boundary are usually not as good as those inside and could be sold as lower-frequency chips. The industry is pursuing the next step of 450-mm wafers, which will greatly increase the yield but would require an even larger uniform plasma.

The structure of a transistor is shown in Fig. 10.67. Its function is to control an electrical current with a gate that requires very little power, just as a dam can control a large amount of hydro power by opening and closing an actual gate. In

Fig. 10.67 electrons flow from the source S to the drain D, so that the positive current I_D goes from D to S. The current is controlled by the voltage V_G, which is capacitively coupled through an insulator to change the width of the current channel.

To make such transistors requires a series of steps of masking, etching, and deposition. Silicon can be etched chemically with chlorine or fluorine, or physically with energetic beams of atoms or ions. Winters and Coburn showed that silicon can be etched with XeF_2, a gas, but that the etch rate is greatly enhanced by Ar^+. Their famous graph is shown in Fig. 10.68. With only XeF_2 or with only an argon ion beam accelerated through the sheath, the etch rate is more than an order of magnitude lower than with both. This effect has been explained by molecular dynamics simulations by David Graves. By following the motion of each atom in a surface layer of hydrogenated amorphous carbon, he showed, in Fig. 10.69, that an argon ion beam sputters away the H atoms near the surface to a depth increasing with A^+ energy.

The patterns of Fig. 10.67 are built up layer by layer with photolithography, a process shown in Fig. 10.70. A photoresist layer is sensitive to UV light and areas exposed to light can be chemically dissolved or retained. The resist blocks the etching beams so that the desired pattern is etched in the Si layer underneath. The resist is then dissolved away. Figure 10.71 shows the etching process. A plasma containing Cl, F, and Ar ions and neutrals is at the top, and ions are accelerated by the sheath potential down to the substrate. At the top of each column is the mask protecting the layers below it.

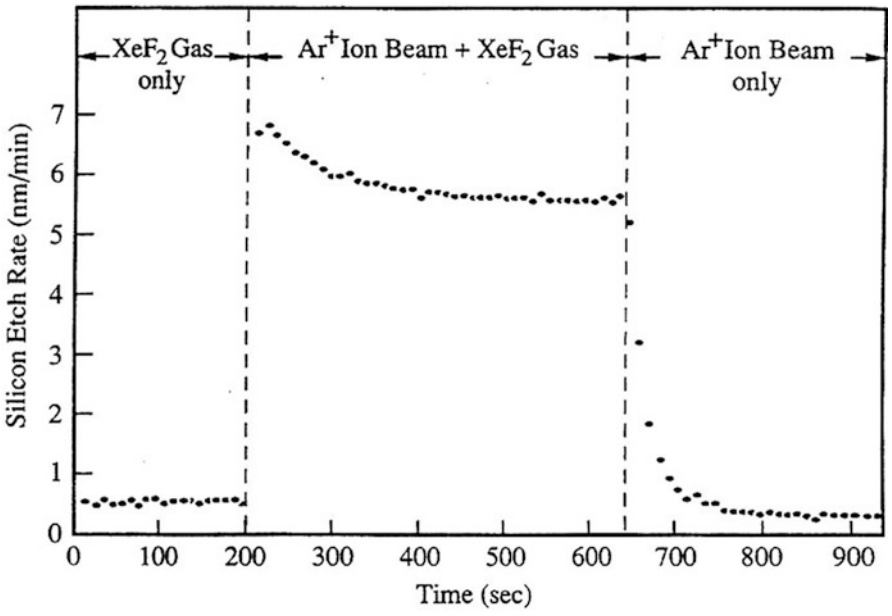

Fig. 10.68 The Coburn graph of symbiotic etching

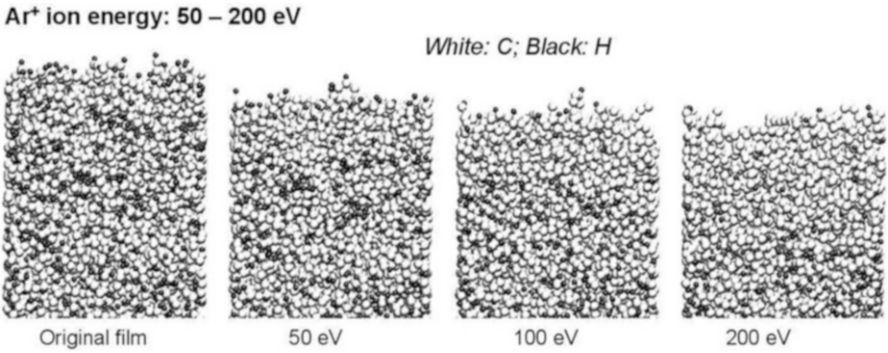

Fig. 10.69 Molecular dynamics simulation of an aC-H (hydrogenated amorphous carbon) layer bombarded by argon ions at various energies [D.B. Graves, Gaseous Electronics Conference, 2011]

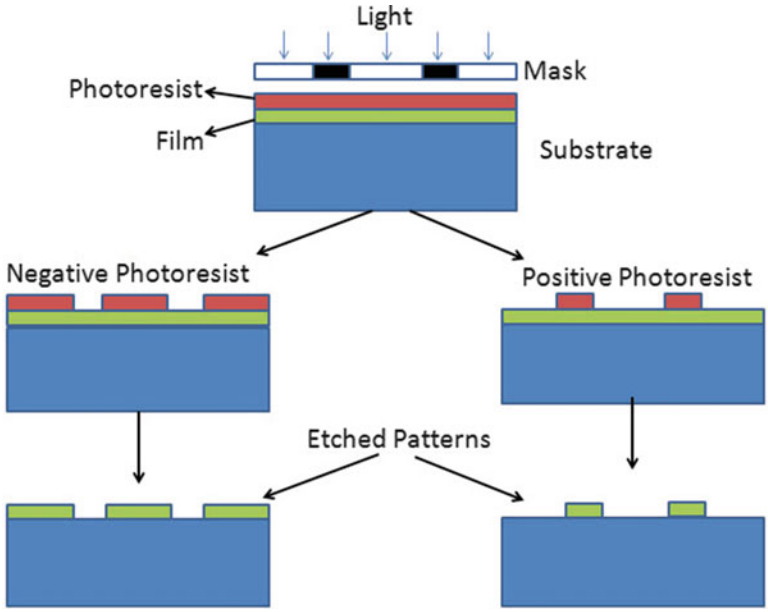

Fig. 10.70 Patterning by photolithography

The patterning of transistors requires light of wavelengths shorter than critical dimensions of their features. As the CDs got smaller, ultraviolet light from excimer lasers had to be used. This involved new optics that can pass UV. Eventually, shorter wavelengths in the X-ray range will be needed. In that case, only reflective optics can be used, and this will require development of new technology. We have a long way to go, however, to duplicate the computing ability of the human brain with an instrument of that size.

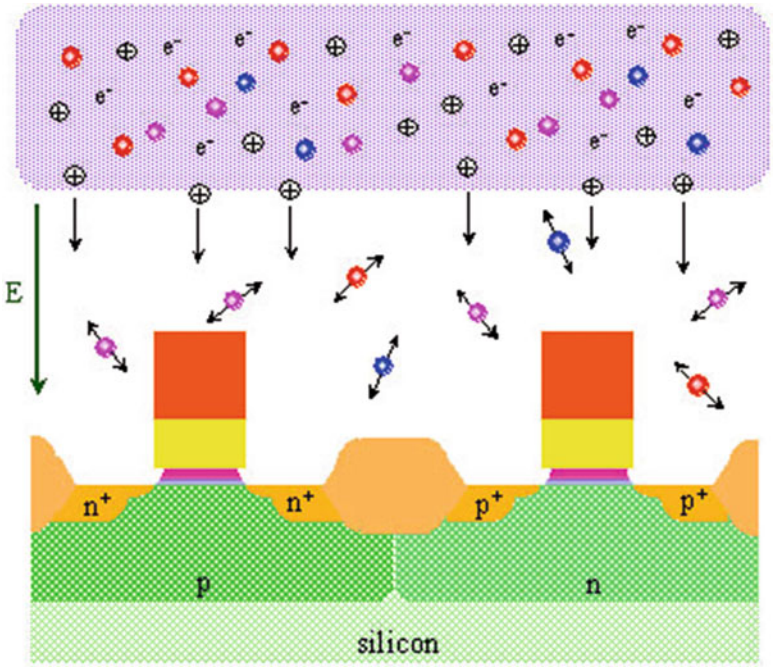

Fig. 10.71 Cartoon of semiconductor etching. The *top layer* of the columns is the mask

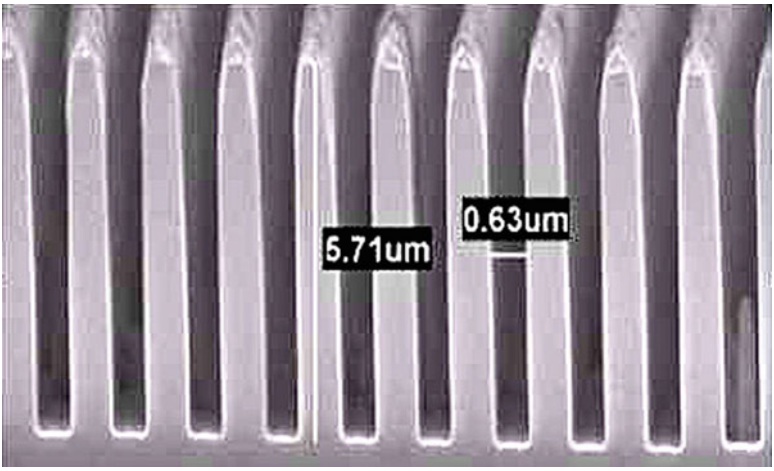

Fig. 10.72 Trenches formed with Deep RIE

When a deep trench or via is required, a process called DRIE (Deep Reactive Ion Etching, Fig. 10.72) is used. To keep the trench straight, etching and passivation are applied alternately. Etching is done with, say, SF_6; and, after a few seconds, an inert

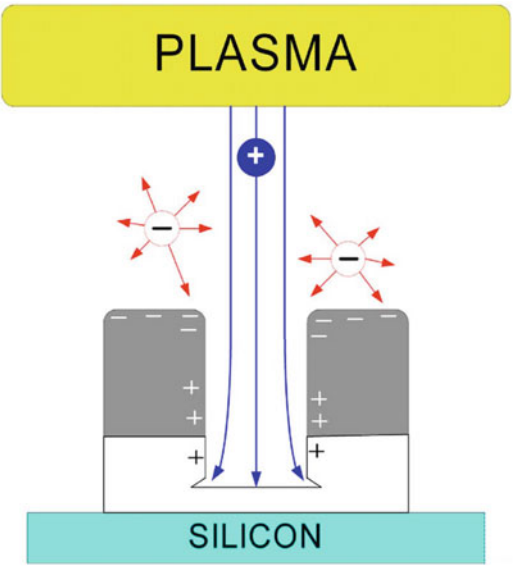

Fig. 10.73 Notches at the bottom of a trench

passivation layer like teflon is laid on with C_4F_8. This protects the walls, but the etching ions can cut through it at the bottoms to allow chemical etching to occur. This is sometimes called the Bosch process.

The bottoms of the trenches can have defects, such as notches or micro-trenches. Notches can form from bombardment by ions with curved trajectories. In Fig. 10.73 the thick shaded layer at the top is the mask, which is charged negatively at the top by electrons, which attract the ions, bending them towards the wall. The bottom of the trench is charged positively by ions which have collected on the wall. The resulting electric fields determine the ion trajectories which etch the notches at the bottom. Figure 10.74 shows an SEM (Scanning Electron Microscope) image of an actual trench deformed with microtrenches.

The mask shown in Fig. 10.73 is shown with rounded edges. Since the charges that build up on these edges create E-fields, the ion orbits vary with these charges. An example is shown in Fig. 10.75. This computation compares ion orbits with sharp trench entrances with those with rounded ones, taking into account the surface charges. A sharp edge shields ions from the sidewalls, whereas even a slight rounding of the edge allows ions to deposit positive charge to the wall. A more obvious electron shielding effect also occurs, with surface electron charges repelling electrons from the nanometer-size trench.

This was a brief glimpse of the complex technology that makes modern electronics possible.

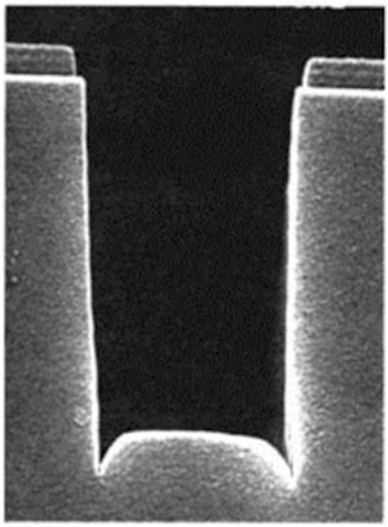

Fig. 10.74 Micro-trenches at the bottom of a trench [R. J. Hoekstra, M.J. Kushner, V. Sukharev, and P. Schoenborn, J. Vac. Sci. Technol. B **16**, 2102 (1998)]

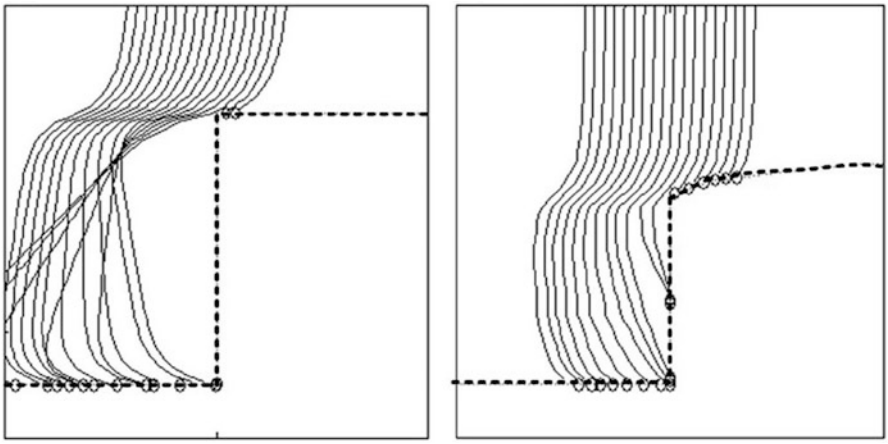

Fig. 10.75 Deflections of the orbits of ions from the plasma at the top caused by surface charges on the mask, for a square trench entrance (*left*), and a rounded one (*right*) [T.G. Madziwa-Nussinov, D. Arnush, and F.F. Chen, Phys. Plasmas **15**, 013503 (2008)]

10.6 Spacecraft Propulsion

10.6.1 General Principles

Once a satellite has been put into orbit, it needs a small amount of thrust once in a while to keep it there or to change its orbit. Chemical thrusters were formerly used but have been largely replaced by more efficient ion thrusters. These are of three

kinds: gridded thrusters, Hall effect thrusters (HETs), and the new helicon thrusters, still under development. Ion thrusters are characterized by their *specific impulse* $I_{\rm sp}$, defined by

$$I_{sp} \equiv v_{ex}/g \text{ sec}, \tag{10.22}$$

where $v_{\rm ex}$ is the exhaust velocity of the rocket, and g is the acceleration of gravity, of magnitude 9.8 m/s. Note that $I_{\rm sp}$ has the units of seconds. What this means physically is that if a rock is dropped from a height, it will reach the velocity $v_{\rm ex}$ in $I_{\rm sp}$ seconds.

The total amount of thrust is limited by the amount of mass available for ejection. Let M be the total mass of the load consisting of the intrinsic spacecraft mass $m_{\rm s}$ plus the decreasing propellant mass $m_{\rm p}$:

$$M(t) = m_s + m_p(t). \tag{10.23}$$

In the frame of the spacecraft, its velocity v is zero, and its acceleration dv/dt is positive. The thrust T is the negative of the rate of change of exhaust momentum:

$$T = -\frac{d}{dt}\left(m_p v_{ex}\right) = -v_{ex}\frac{dM}{dt}. \tag{10.24}$$

The spacecraft's acceleration due to T is given by

$$T = \frac{d}{dt}(Mv) = M\frac{dv}{dt}, \tag{10.25}$$

$$\frac{dv}{dt} = -v_{ex}\frac{1}{M}\left(\frac{dM}{dt}\right) = -v_{ex}\left[\frac{d(\ln M)}{dt}\right]. \tag{10.26}$$

Integration from the initial velocity $v_{\rm i}$ to the final one $v_{\rm f}$ as $m_{\rm p}$ goes from $m_{\rm p0}$ to 0 gives

$$\int_{v_i}^{v_f}\frac{dv}{dt}dt \equiv \Delta v = -v_{ex}\int_{M_i}^{M_f}\frac{d(\ln M)}{dt}dt = -v_{ex}\ln\left(\frac{m_s}{m_s + m_{p0}}\right). \tag{10.27}$$

The mass of propellant needed for a given Δv is then

$$m_{p0} = m_s\left(e^{\Delta v/v_{ex}} - 1\right). \tag{10.28}$$

The amount of propellant needed to accelerate a given mass to a given velocity depends exponentially on the exhaust velocity $v_{\rm ex}$.

10.6.2 Types of Thrusters

10.6.2.1 Gridded Thrusters

A schematic of a gridded thruster is shown in Fig. 10.76. A plasma is created by a voltage applied between a cathode and an anode grid. The cathode could be a good electron emitter like lanthanum hexaboride (LaB_6). Electrons are retained and ions are accelerated by grids. The ion beam will not detach from the spacecraft unless it is neutralized, so electron emitters have to be added at the sides to inject electrons into the accelerated ion beam and prevent the spacecraft from charging to a high negative potential. The neutralizers are usually hollow-cathode discharges. The ejected plume of plasma can then be formed by nozzles into an optimal shape. Sputtering limits the lifetime of the grids, but they have been designed to last at least 30,000 h.

10.6.2.2 Hall Thrusters

Elements of a Hall thruster are shown in Fig. 10.77, which is a cross section of a cylindrically symmetric device. A plasma is formed between the coaxial cylinders by applying a high voltage to the anode ring at the left. This voltage accelerates the

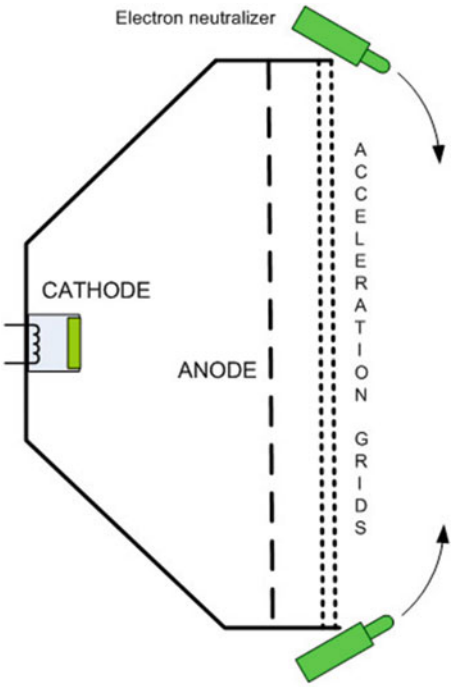

Fig. 10.76 A gridded ion thruster

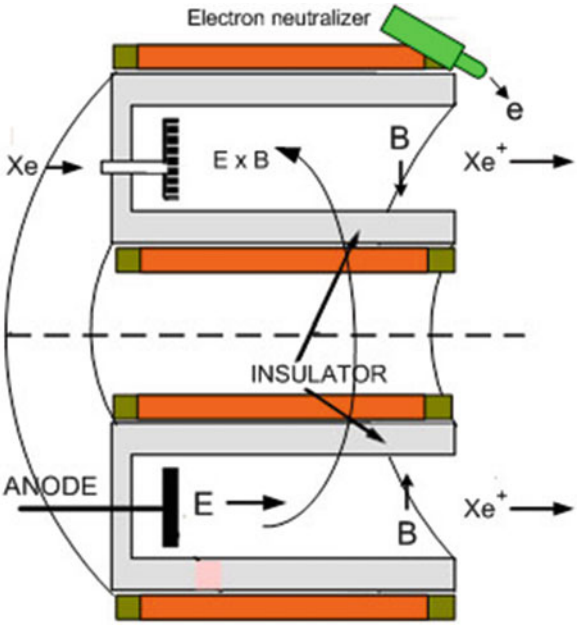

Fig. 10.77 A Hall effect thruster

ions to v_{ex}. Holes in the ring also serve as the gas feed, as shown in the upper cross section. Xenon is normally used because of it is an inert, monatomic gas with high mass and low ionization potential. A radial magnetic field is created by coils (not as shown) in order to prevent electrons from following the ions. The electrons instead drift azimuthally with their $\mathbf{E} \times \mathbf{B}$ drift, forming the Hall current. Here again, electron neutralizers have to be added to neutralize the ejected ion beam. The function of the magnetic field is to prevent the electrons from moving axially and collapsing the anode voltage into a thin sheath at the anode. Hall thrusters have a few intrinsic problems. One is secondary emission of cold electrons from the internal surfaces which can upset the charge balance in the plasma. This can be minimized by coating the surfaces with carbon velvet. A second problem is instability, since many types of instabilities arise when there is a magnetic field (B-field). In spite of these problems, Hall thrusters have been engineered successfully to fly in space.

10.6.2.3 Helicon Thrusters

Helicon plasmas, described in Sect. 9.5, could be advantageous for thrusters because of their high ionization efficiency and their thrust without an auxiliary E-field. Elements of a helicon thruster are shown in Fig. 10.78. The required DC magnetic field is generated by coils surrounding the tube. The RF is applied to an antenna, shown here as one side of a Boswell antenna, which is a version of the bidirectional Nagoya Type III antenna. Helical antennas can couple more

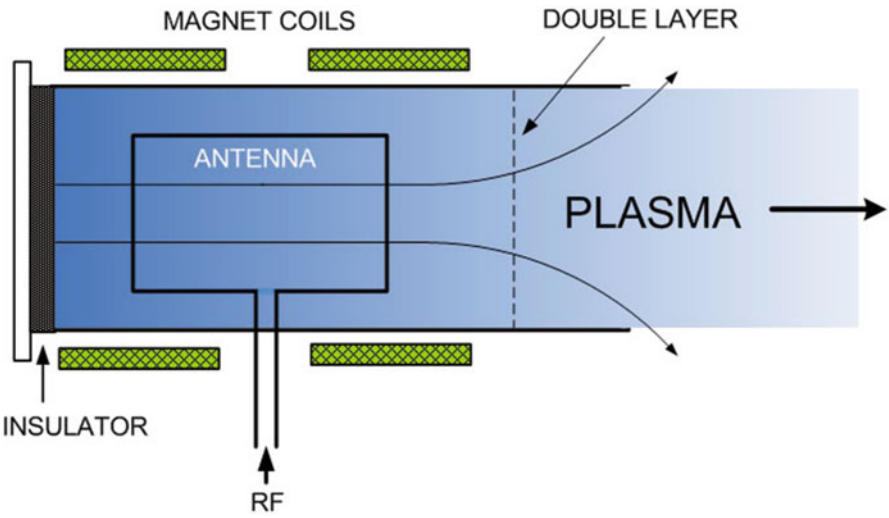

Fig. 10.78 Schematic of a helicon thruster [Drawn after C. Charles, J. Phys. D: Appl. Phys. **42** (2009) 163001]

efficiently to the dominant $m = +1$ azimuthal mode of the helicon wave, and ring antennas are used for the $m = 0$ mode. As the plasma leaves the uniform-field volume, the field lines diverge as the B-field expands. The electrons follow the field lines, and hence their density decreases. Since the electrons are essentially Maxwellian, the plasma potential must decrease with the density according to Eq. (3.73). There is therefore an electric field along the field lines shown in Fig. 10.78. This E-field accelerates ions; and, if $T_i \approx 0$, the ion velocity will eventually reach the acoustic velocity c_s. At that point, a sheath will form, according to Fig. 8.4, whether or not there is a wall there. This ion-rich sheath in "mid-air" will attract electrons which surround it, forming a *double layer* which, in 1D, shields the E-field from the rest of the plasma.

It is possible to calculate where this double layer will form. The ion energy at the sheath edge is $\frac{1}{2}Mc_s^2 = \frac{1}{2}KT_e$. To accelerate ions to this energy, the potential at the sheath edge, V_s, must be at least $-\frac{1}{2}KT_e/e$ if $V_s \equiv 0$ in the main plasma. Hence, the quasineutral density at the sheath edge, n_s, is given by Eq. (3.73) as

$$n_s = n_0 \exp(-\tfrac{1}{2}). \tag{10.29}$$

Since magnetic flux is conserved in the expansion from r_0 to r for each field line, and since electrons are constrained to follow the field lines, the field and density vary with r as

$$\frac{B}{B_0} = \frac{n}{n_0} = \left(\frac{r_0}{r}\right)^2. \tag{10.30}$$

The radius at which a sheath forms is then

$$\frac{r_s}{r_0} = \left(\frac{n_0}{n_s}\right)^{1/2} = e^{1/4} = 1.28. \tag{10.31}$$

Thus, an ion sheath will form at a position where the field lines have increased their distances from the axis by 28%. Ions passing through the potential drop of this sheath are suddenly accelerated to a velocity v_{ex} of Eq. (10.22).

Helicon thrusters have been tested in space but have not been fully engineered. Nonetheless, helicon discharges are part of the large thruster VASIMR (Variable Specific Impulse Magnetoplasma Rocket) being built by former astronaut Franklin Chang Díaz for travel to Mars. A diagram of this device is shown in Fig. 10.79. Though helicons are used for ionization, the main power is provided by ICRH (see section "Heating and Current Drive").

There will not be a more glamorous application of helicons!

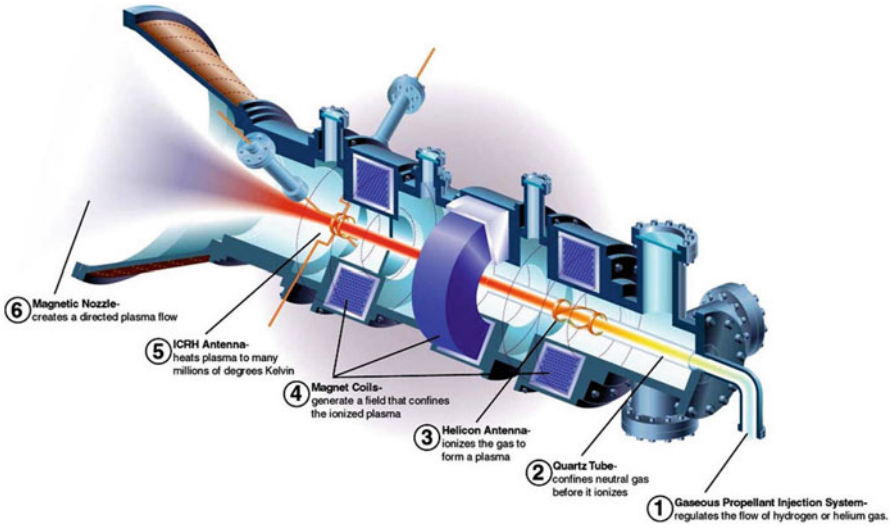

Fig. 10.79 The VASIMR rocket [Google images]

10.7 Plasmas in Everyday Life

Plasma physics may be an obscure and difficult science, but it is important because we see plasmas all the time. Every time we turn on the television, there are plasmas inside every pixel. Even before that, when we turn on the fluorescent lights, we are using a plasma. Older computer screens are also lit by fluorescents. The light of day is caused by the plasma in the sun's photosphere. Moonlight is a reflection of that. At night, the stars and nebulas can be seen by their plasma light. Without plasma, it would be very dark. Auroras are plasmas generated by the solar wind. When we get a shock when touching a doorknob after walking across a rug in winter, the spark is a plasma. Lightning is a larger form of that, coming from clouds. Ball lightning, though, is a slow-moving ball of plasma that no one understands.

We conclude with the topic that engendered plasma physics: nuclear fusion, which the general public has never heard of. By about 2050, there will be very little fossil fuel left; maybe dirty coal, but certainly not oil. Wind, solar, and hydro power are insufficient for the world's growing energy needs. Nuclear (fission) energy has its well known problems. To survive at least a few more centuries, mankind has to develop fusion power. This will require a workforce trained in plasma physics. The control of global warming starts in the classroom.